Swiss J Geosci (2017) 110:479–501
DOI 10.1007/s00015-016-0239-y

Zircon U–Pb geochronology of lower crust and quartzo-feldspathic clastic sediments from the Balagne ophiolite (Corsica)

Maria Rosaria Renna[1] · Riccardo Tribuzio[2,3] · Alessio Sanfilippo[2,3] · Massimo Tiepolo[4]

Received: 1 June 2016 / Accepted: 9 December 2016 / Published online: 2 March 2017

Abstract The Balagne ophiolite from central-northern Corsica represents a continent-near paleogeographic domain of the Jurassic Liguria-Piedmont ophiolitic basin. Pillow and massive basalt lavas are primarily associated with Middle–Upper Jurassic pelagic sediments (mostly radiolarites at their base), continental-derived quartzo-feldspathic clastic sediments and ophiolitic breccias containing clasts of gabbros and basalts. The basalt-sedimentary succession is tectonically associated with a slice composed of an intrusive sequence overlain by basalt lavas. A "plagiogranite" from the intrusive sequence was dated by U–Pb zircon geochronology. Although affected by some uncertainty, mainly reflecting common Pb contamination, the U–Pb zircon data suggest a crystallization age of 159 ± 3 Ma (MSWD = 6.3), which is coeval with the formation of oceanic lower crust in the Schistes Lustrés units from Alpine Corsica. The predominance of quartz grains preserving typical volcanic shape, the prevalence of prismatic zircons and the arkose whole-rock composition indicate that the continental-derived quartzo-feldspathic clastic sediments have a low degree of textural maturity. U–Pb zircon geochronology carried out on two distinct levels of quartzo-feldspathic clastic sediments identified the predominance of zircons with within error U–Pb dates at ~280 Ma; minor components at ~457, ~309 and ~262 Ma were also obtained. The U–Pb date distribution is consistent with a source magmatic material mostly developed during the Variscan orogenic collapse.

Keywords Alpine Corsica · Jurassic ophiolites · Basalt-sedimentary succession · U–Pb zircon geochronology · Formation of oceanic gabbroic crust

Editorial handling: C. Sue and S. Schmid.

✉ Maria Rosaria Renna
mrenna@unime.it

[1] Dipartimento di Scienze Matematiche e Informatiche, Scienze Fisiche e Scienze della Terra, Università di Messina, Viale F. Stagno D'Alcontres 31, 98166 Messina, Italy

[2] Dipartimento di Scienze della Terra e dell'Ambiente, Università di Pavia, Via Ferrata 1, 27100 Pavia, Italy

[3] C.N.R.-Istituto di Geoscienze e Georisorse, U. O. di Pavia, Via Ferrata 1, 27100 Pavia, Italy

[4] Dipartimento di Scienze della Terra "Ardito Desio", Università di Milano, via Botticelli 23, 20133 Milan, Italy

1 Introduction

The Jurassic Alpine ophiolites (Fig. 1a) are considered the lithospheric remnants of an (ultra-) slow spreading ocean called Liguria-Piedmont basin, which was located between the Europe/Corsica and Adria continental margins (e.g., Lagabrielle and Cannat 1990). Some of the ophiolitic bodies from the Alpine-Apennine belt are characterized by oceanic crust associated with continental crust material (Manatschal and Nievergelt 1997; Marroni et al. 1998; Beltrando et al. 2014) and/or mantle sequences retaining a subcontinental lithospheric origin (Rampone et al. 1995; Müntener et al. 2004; Montanini et al. 2006). These ophiolites are considered fossil analogous of modern magma-poor ocean-continent transition domains (e.g., Manatschal and Müntener 2009). The Balagne ophiolitic nappe from central-northern Corsica is characterized by the primary Jurassic association of pillow and massive basalt lavas with gabbro-basalt breccias and pelagic sediments (mostly radiolarites). The Balagne basalt lavas include quartzo-feldspathic clastic sediments of continental origin indicating proximity to a continental margin (Baud and

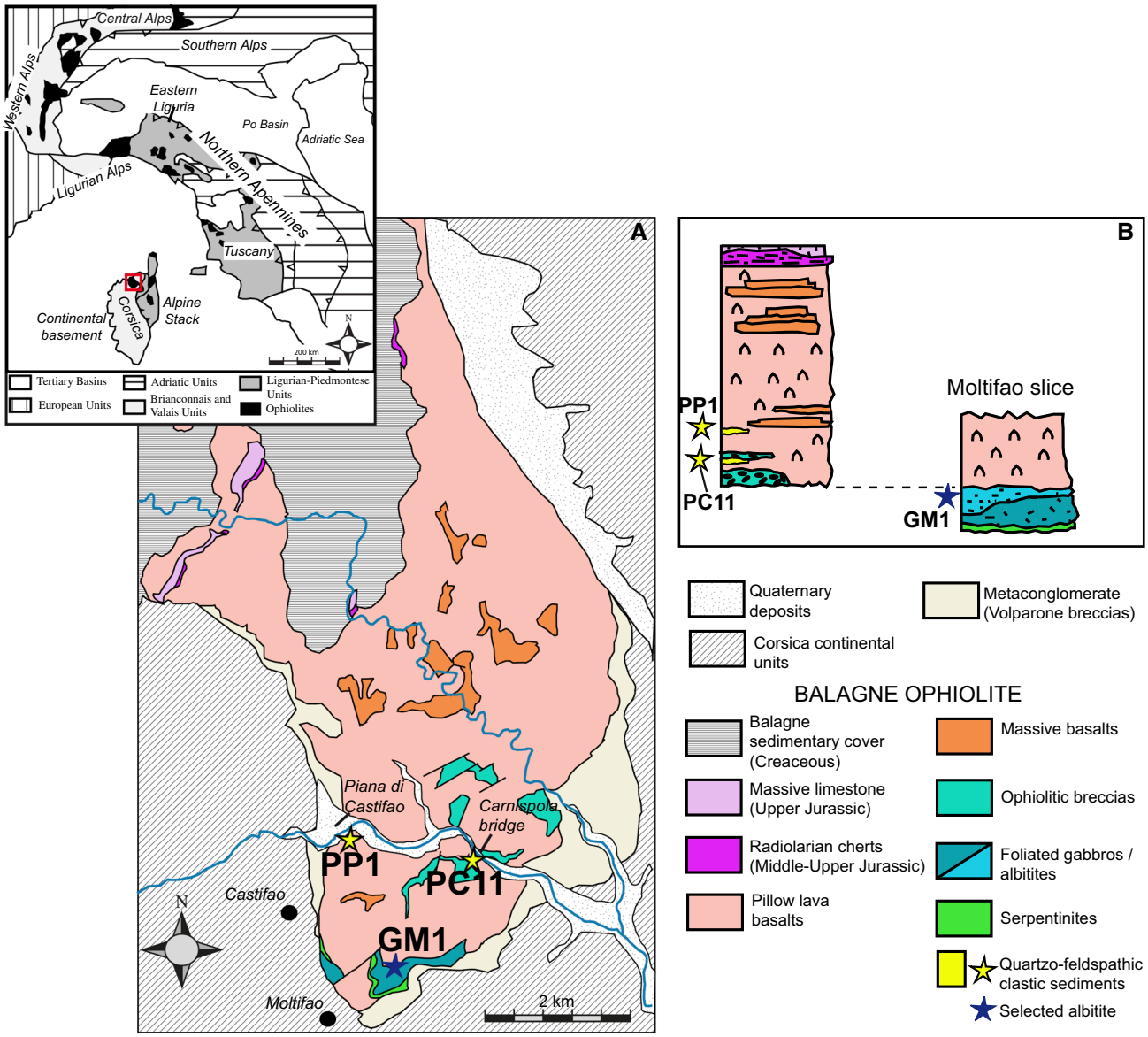

Fig. 1 **a** Geological map of the Balagne ophiolite (redrawn after Rossi et al. 2001) and geographical location of the ophiolites of Corsica island (inset map). **b** Stratigraphic reconstruction of the Balagne volcano-sedimentary sequence and location of sample selected for the geochronological investigation. A simplified reconstruction of the Multifao slice (not to scale) is also shown. The two sections are correlated assuming that the gabbros in the lowermost part of the Multifao slice represent the substrate of the Balagne ophiolite

Rollet 1973; Durand-Delga et al. 1997; Rossi and Durand-Delga 2001; Rossi et al. 2002; Marroni and Pandolfi 2003; Bracciali et al. 2007). Whether the Balagne ophiolitic nappe originated from proximity to the European continent, near the margin of the Corsica-Sardinia block, or to the Adria paleo-margin is still a matter of debate (see also Malavieille et al. 1998; Molli 2008; Li et al. 2015).

Previous geochemical studies showed that the basalts from the Balagne area have transitional mid-ocean ridge affinity, exemplified by slight enrichment of LREE relative to MREE and HREE in their REE patterns (e.g., Venturelli et al. 1979). This geochemical characteristic was attributed to crustal contamination (Durand-Delga et al. 1997) or an origin from a lithospheric mantle source (Saccani et al. 2008). The REE signature of the basalts from the Balagne ophiolite has been recently interpreted to reflect the presence of garnet in the mantle source (Saccani et al. 2015). Rossi et al. (2002) proposed an U–Pb zircon age of 169 ± 3 Ma for the formation of the lower crust in the Balagne ophiolite. This is the oldest U–Pb zircon age reported in the literature for the lower crust sequences of the Alpine-Apennine ophiolites, which mostly range between 166 and 158 Ma (Fig. 2; Bill et al. 1997; Rubatto et al. 1998; Rossi et al. 2002; Schaltegger et al. 2002;

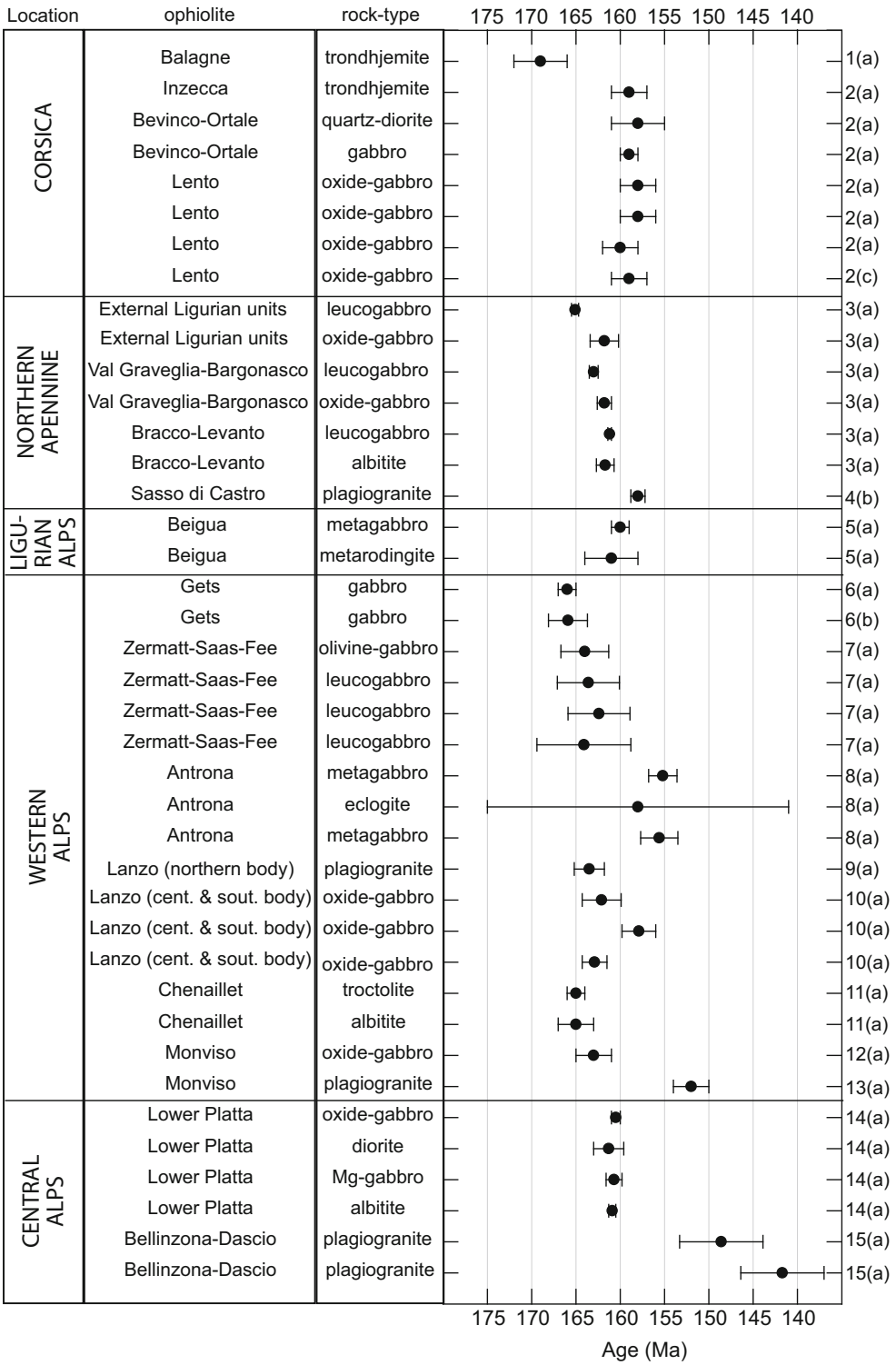

Fig. 2 Available geochronological data for the intrusive rocks from the Jurassic ophiolites of the Alpine-Apennine belt. Data sources: 1, Rossi et al. (2002); 2, Li et al. (2015); 3, Tribuzio et al. (2016); 4, Bortolotti et al. (1995); 5, Rubatto and Scambelluri (2003); 6, Bill et al. (1997); 7, Rubatto et al. (1998); 8, Liati et al. (2005); 9, Rubatto et al. (2008); 10, Kaczmarek et al. (2008); 11, Li et al. (2013); 12, Rubatto and Hermann (2003); 13, Lombardo et al. (2002); 14, Schaltegger et al. (2002); 15, Stucki et al. (2003). Methods used: (**a**), U–Pb zircon age; (**b**), $^{40}Ar/^{39}Ar$ amphibole plateau age; (**c**), U–Pb baddeleyite age. U–Pb zircon ages acquired by conventional isotope dilution TIMS for felsic rocks by Ohnenstetter et al. (1981), Borsi et al. (1996) and Costa and Caby (2001) are not reported

Rubatto and Scambelluri 2003; Rubatto and Hermann 2003; Rubatto et al. 2008; Kaczmarek et al. 2008; Li et al. 2013, 2015; Tribuzio et al. 2016). Indeed, relatively young U–Pb zircon dates (~156 to ~142 Ma) were obtained for few meta-gabbros and meta-plagiogranites from the ophiolites of the Western and Central Alps, which show extensive metamorphic recrystallization in response to the Alpine orogenic cycle (Liati et al. 2005; Lombardo et al. 2002; Stucki et al. 2003). These U–Pb zircon dates may be affected by radiogenic Pb loss in response to Alpine metamorphism and are therefore considered not to be robustly constrained (Li et al. 2013; Tribuzio et al. 2016).

The U–Pb zircon age obtained by Rossi et al. (2002) is associated with a high MSWD (8.4, $N = 11$), thereby implying age dispersion outside the analytical uncertainties, with the data involving more than one statistically valid population. No geochronological constraints are available for the source rocks of the quartzo-feldspathic sediments. Zircons from Balagne quartzo-feldspathic sediments were studied from a morphological viewpoint and were related to a continental source material mostly made up of granitoids similar to the Upper Carboniferous-Lower Permian hornblende granitoids from the Corsica batholith (Durand-Delga et al. 1997; Rossi and Durand-Delga 2001).

The main aim of this study is to provide new geochronological constraints to better assess (1) the age of the lower crust from the Balagne ophiolite, and (2) the source of the quartzo-feldspathic deposits interspersed within the Balagne basalt lavas. New field observations have been therefore coupled with geochronological investigations carried out on gabbroic rocks and quartzo-feldspathic sediments. In particular, in situ U–Pb zircon determinations were obtained for two samples of quartzo-feldspathic sediments and a "plagiogranite" from the intrusive gabbroic sequence. The data allowed us to shed new light on the formation of the Corsican segment of the Jurassic basin.

2 Geological framework

The Balagne ophiolite represents a Jurassic ophiolitic sequence and its Middle Jurassic-Upper Cretaceous sedimentary cover (Durand-Delga 1984). The ophiolite is a crustal fragment of the Liguria-Piedmont basin (Durand-Delga et al. 1997), which was unaffected by the high pressure/low temperature metamorphism typical of most tectonic units from the Schistes Lustrés units (e.g., Molli and Malavieille 2011). The Balagne ophiolite is located at the top of Alpine Corsica stack (Marroni and Pandolfi 2003).

The Balagne ophiolite (Fig. 1) mainly consists of pillow basalts locally interlayered with levels of massive basalts and deposits of ophiolitic breccias (Baud 1975; Gruppo di Lavoro sulle Ofioliti Mediterranee 1977; Durand-Delga et al. 2001; Rossi et al. 2001). Gabbros and/or serpentinites were considered to form the substrate of the basaltic sequence (see also Rossi et al. 2001), with the serpentinites suggested to derive either from plagioclase-peridotites (Baud 1975) or olivine-gabbros (Durand-Delga et al. 2001).

The ophiolitic breccias from the Balagne ophiolite contain clasts of gabbros and basalts embedded in a matrix mostly composed of gabbro and basalt fragments. The matrix locally shows internal, graded bedding and/or sedimentary structures (Marroni et al. 2007). The oxide-gabbro clasts are locally crosscut by leucocratic felsic dykes. SHRIMP U–Pb zircon geochronology (Rossi et al. 2002) was carried out for a leucocratic felsic dyke crosscutting an oxide-rich gabbro clast from the gabbro-basalt breccias. The SHRIMP analyses gave mostly discordant $^{206}Pb/^{238}U$ and $^{207}Pb/^{235}U$ dates; the $^{206}Pb/^{238}U$ dates range from 175 ± 3 (2σ) to 163 ± 3 Ma (2σ) and yield a lower intercept of 169 ± 3 Ma (2σ, MSWD = 8.4, $N = 11$). This date was interpreted as the age of crystallization of the gabbroic sequence. A slightly younger concordant zircon with a $^{206}Pb/^{238}U$ age of 156 ± 2 Ma (2σ) was also found and interpreted to have experienced radiogenic Pb loss. A discordant zircon with a $^{206}Pb/^{238}U$ age of 431 ± 8 Ma (2σ) and a concordant zircon with a U–Pb concordant age of 2705 ± 21 Ma (2σ) were also found and interpreted to be inherited grains.

In the lower stratigraphic portion of the Balagne ophiolitic sequence, a level of quartzitic sandstone intercalated within pillow basalts was documented near Piana di Castifao (Fig. 1; Baud 1975; Durand-Delga et al. 1997; Peybernès et al. 2001; Rossi and Durand-Delga 2001). The quartzitic sandstone has calcareous cement and shows graded-bedding indicated by grain size variation and the occurrence of mm-thick bands of mica-bearing pelites. In the proximity of the contact with the pillows, the sandstone contains fragments of micaschist and basalt. On the basis of a morphological study (Durand-Delga et al. 1997; Rossi and Durand-Delga 2001), the detrital zircons from this quartzitic sandstone level were interpreted to derive from the Upper Carboniferous hornblende granitoids from the Corsica batholith. The Balagne ophiolite was therefore interpreted to represent a sector of the Jurassic Liguria-Piedmont basin located close to the European continent (see also Marroni and Pandolfi 2003). Conversely, other authors considered the Balagne ophiolite as a relic of an intraoceanic accretionary wedge formed by offscrapping and shallow underplating of a sector of the basin originally

located towards the Adria margin (Malavieille et al. 1998; Molli 2008).

At the stratigraphic top of the Balagne ophiolitic sequence, the pillow basalts are covered by a Middle–Upper Jurassic sedimentary sequence mainly made up of radiolarian cherts, which grade upward into Cretaceous Calpionella limestones and Palombini shales (Marroni and Pandolfi 2003). Radiolarian cherts are up to 10–30 m thick, but in places their thickness is reduced or even absent (Danelian et al. 2008). The Calpionella limestones are locally overlain by a sequence of massive calcarenite-breccia containing fragments of volcano-clastic material, granites and metamorphic rocks, which were interpreted to derive from the Corsica batholith (Durand-Delga et al. 1997). The oldest radiolarian cherts are Late Bathonian to Early Callovian in age (Chiari et al. 2000; Bill et al. 2001; Peybernès et al. 2001; Danelian et al. 2008).

3 New field data

In the southern sector of the Balagne ophiolite the pillow basalts are overthrust by a tectonic slice (see also Rossi et al. 2001) that we term Moltifao slice. This slice (~100 m in thickness) consists of a mafic sequence showing, at the base, a 5–10 m-thick level of serpentinites, which locally include domains preserving a plagioclase-rich gabbroic protolith. The serpentinites (Fig. 1) are stratigraphically overlain by decametric thick levels of evolved gabbros (gabbronorites to oxide-rich gabbros) that are in turn followed by quartz-free leucocratic rocks mostly consisting of plagioclase (hereafter referred to as albitites). The evolved gabbros and the overlying albitites exhibit a magmatic foliation locally overprinted by a tectonic foliation. The Moltifao mafic sequence is topped by pillow lava basalts. Close to the basalts, the albitites show a reddish color that is probably related to late development of hematite along grain boundaries and micro-fractures.

With the exception of the Moltifao slice, many of the exposures previously described as gabbros in the lower part of the Balagne ophiolitic sequence (Rossi et al. 2001) are considered to be ophiolitic gabbro-rich breccias. These breccias mainly occur within the pillow basalts at the base of the Balagne ophiolitic sequence. The clasts mainly consist of undeformed clinopyroxene-rich gabbros ranging from some decimeters to a few meters in size. Clasts of clinopyroxene-rich sheared gabbros, nearly undeformed gabbronorites to oxide-rich gabbros, pillow basalts and leucocratic felsic rocks are also present (overall a few decimeters in size).

Next to the Carnispola bridge, a new quartzo-feldspathic breccia level (~1 m thick) has been found. The level is mainly composed of feldspars and rounded clasts of quartz (up to 2 mm in size) and is located between a coarse-grained gabbroic breccia at the top and pillow basalts at the base (Fig. 1).

4 Selected samples

Three samples were selected for this study (Table 1): an albitite (GM1) from the Moltifao slice, a quartzo-feldspathic breccia (PC11) from a level located within the ophiolitic breccia near the Carnispola bridge and a sample (PP1) from the quartzitic sandstone level located near Piana di Castifao (cf. Durand-Delga et al. 1997; Rossi and Durand-Delga 2001).

The albitite GM1 is medium-grained and mostly composed of euhedral to subhedral Na-rich plagioclase, which is partly replaced by fine-grained aggregates of secondary albitite + epidote ± chlorite ± white mica. Subhedral to anhedral amphibole occurs in minor modal proportion and is replaced by chlorite + epidote + sphene. Accessory zircon and apatite are also present.

The quartzo-feldspathic breccia PC11 consists of clastic material within a microcrystalline siliceous matrix. The clasts are medium to coarse grained (1 to 5 mm) and mainly composed of sharp feldspars locally showing a prismatic habit (25 vol%) and quartz (20 vol%). The quartz is typically monocrystalline with engulfed shape. Irregular quartz clasts with undulatory extinction and partially recrystallized to fine-grained aggregates are also locally present. Feldspars, dark mica, zircon and apatite are locally included within quartz. Fine-grained clasts of altered dark mica also occur.

The quartzitic sandstone PP1 contains fine-grained (up to 2 mm) clasts of quartz (30 vol%), feldspars (25 vol%) and calcite (25 vol%) within a calcite-rich microcrystalline matrix. The quartz clasts typically consist of engulfed monocrystalline grains, locally containing zircon inclusions (Fig. 3). Sharp polygonal aggregates of quartz are also present. Calcite occurs as irregular clasts and, in places, as rounded to elongated organic shell fragments. Similar fragments were described by Rossi et al. (2001) as crinoids and foraminifera. We also found rare white mica clasts.

Feldspars from both the quartzo-feldspathic breccia and the quartzitic sandstone are typically replaced by fine-grained aggregates made up of albite + white mica ± epidote ± calcite. Dark mica is replaced by fine-grained aggregates consisting of chlorite + white mica + titanite.

5 Analytical procedures

Whole rock major and trace element analyses of the albitite and the quartzo-feldspathic clastic sediments (Table 2) were carried out at Activation Laboratories LTD (Ancaster, Ontario) by inductively coupled plasma (ICP) optical

Table 1 Modal compositions (vol.%) and petrographic features of the selected samples, obtained by visual estimates

Sample	Rock-type	Locality	Latitude and longitude	Pl	Amp	Zrn	Ap		Pl secondary transformation	Amp secondary transformation
GM1	Albitite	Moltifao slice	42°29′43″N 9°07′22″E	95	5	tr	tr		++	+++
				Clasts (vol%)				Matrix (vol%)	Remarks	
PP1	Quartzitic sandstone	Piana di Castifao	42°30′59″N 9°07′21″E	Qtz	Feldspars	Cc		20	15 vol% of Cc clasts are of organic origin	
				30	25	25				
PC11	Quartzo-feldspathic breccia	Carnispola bridge	42°30′45″N 9°08′44″E	Qtz	Feldspar	Dark mica		50		
				20	25	5				

tr, <4%

Extent of secondary transformation of plagioclase and clinopyroxene: +, ≤30%; ++, 30–90%; +++, ≥90%

Mineral abbreviations after Kretz (1983)

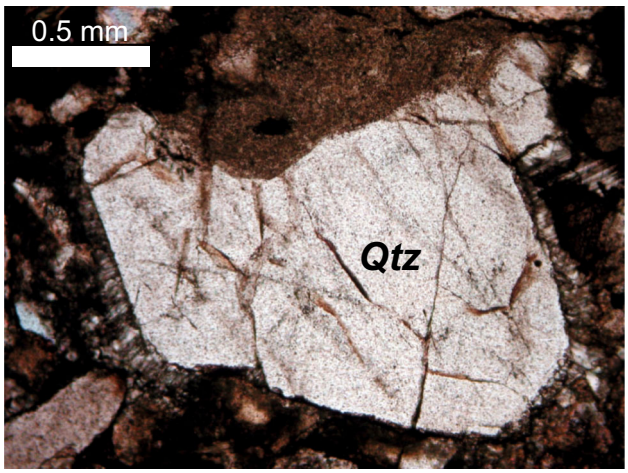

Fig. 3 Thin section photomicrograph of engulfed quartz (Qtz) grain retaining nearly sharp grain boundaries (quartzitic sandstone PP1)

emission spectroscopy and ICP mass spectrometry. Whole rock CO_2 analysis of the quartzitic sandstone was determined at Activation Laboratories LTD (Ancaster, Ontario) by infrared cells with an ELTRA CW-800 analyzer. Details of the analytical techniques and detection limits are available from the company website. In particular, precision and accuracy of trace element analyses are commonly assessed to be within 10%, detection limit of CO_2 analysis is 0.01%.

Zircons were separated from the selected samples using conventional heavy-liquid and magnetic techniques. Representative selections of these minerals, as much as possible free from inclusions and fractures, were extracted by hand-picking under a binocular microscope and mounted in epoxy resin, then polished with ¼ μm diamond paste. Cathodoluminescence (CL) and back-scattered images were used to discern the internal structure of grains, the presence of inclusions and/or altered domains, and to select specific areas for spot analysis. For U–Pb zircon investigation of the quartzo-feldspathic clastic sediments, inherited domains within single grains were not considered.

In situ U–Pb isotope analyses of zircons (Tables 3, 4, 5) were performed at the C.N.R.-Istituto di Geoscienze e Georisorse, Unità di Pavia by laser ablation-ICPMS. The used instrument couples a 193 nm ArF excimer laser (GeoLas102-Microlas) and a high resolution (HR)-ICPMS type Element I from ThermoFinnigan (Table 6). For the present work the laser was operated at a repetition rate of 5 Hz, with a spot diameter of ~20 μm and a laser fluency of 12 Jcm^{-2}. The analytical procedures were basically the same as those described in Tiepolo (2003). Laser-induced U–Pb fractionation and mass bias for zircon analyses were corrected by external standardisation using zircon GJ1 (608.5 ± 0.4 Ma, Jackson et al. 2004). The time-resolved signal was carefully inspected to detect U–Pb isotope heterogeneities within the ablated volume; only homogeneous intervals of at least 25 s were considered. Data reduction, isotope ratio and apparent age calculations were carried out with the IOLITE software (Paton et al. 2011) utilizing the U–Pb geochronology 3 data reduction scheme (Paton et al. 2010). Concordia plot, age probability distribution and weighted average values were calculated using the ISOPLOT/EX software by Ludwig (2003). Data accuracy during analytical runs for zircon was monitored on zircon 91500 (1065 Ma, Wiedenbeck et al. 1995) that yielded results within error of the reference value.

6 Whole-rock compositions

The albitite specimen GM1 has high SiO_2, Al_2O_3 and Na_2O, and low CaO and MgO (Table 2). Its chondrite-normalized REE pattern shows LREE enrichment relative

Table 2 Whole-rock major and trace element compositions of selected samples

Sample rock-type	GM1 albitite	PC11 quartz-rich breccia	PP1 quartzitic sandstone
Major elements (wt%)			
SiO_2	64.8	71.1	54.9
TiO_2	0.21	0.24	0.17
Al_2O_3	18.2	13.6	4.97
$Fe_2O_3^{tot}$	3.36	2.89	0.95
MnO	0.06	0.06	0.05
MgO	0.50	0.69	1.06
CaO	1.50	1.19	20.1
Na_2O	8.97	3.08	1.09
K_2O	0.12	4.56	1.02
P_2O_5	0.03	0.07	0.04
L.O.I	0.85	1.99	16.2
Total	98.6	99.5	100.5
Mg#	22.8	32.1	68.9
CO_2	–	–	15.2
SiO_2/Al_2O_3		5.24	11.0
Trace elements (ppm)			
V	10	17	16
Cr	<20	<20	<20
Sc	<1	5	3
Co	3	3	<1
Cu	160	<10	<10
Zn	30	40	<30
Ga	35	14	5
Sn	6	3	2
Rb	2	196	34
Sr	239	92	111
Ba	20	528	101
Zr	1,990	140	97.0
Nb	15	10.5	3.70
Y	91	27.8	16.4
Hf	44.3	4.30	2.40
Ta	1.80	1.25	0.46
Pb	5	11	12
Th	3.40	15.3	5.87
U	1.90	3.29	2.10
La	25.8	36.0	15.2
Ce	58.9	68.9	26.2
Pr	6.83	7.47	3.21
Nd	26.2	26.0	12.2
Sm	6.70	5.08	2.48
Eu	1.15	0.77	0.46
Gd	7.80	4.49	2.23
Tb	1.70	0.78	0.37
Dy	12.7	4.80	2.33
Ho	3.00	0.99	0.48
Er	10.6	2.96	1.41
Tm	1.90	0.45	0.21
Yb	14.7	3.01	1.38
Lu	2.54	0.50	0.20
La_N/Sm_N	2.41	7.46	6.45
Gd_N/Yb_N	0.44	1.24	1.34
Eu/Eu*	0.48	0.49	0.59

L.O.I. loss on ignition. Mg# = 100 × molar $Mg/(Mg + Fe^{2+}_{tot})$

–, not determined

$Eu/Eu^* = Eu_N/(Sm_N \times Gd_N)^{0.5}$

to MREE and a marked negative Eu anomaly (Fig. 4a). It also shows a significant HREE enrichment relative to MREE, which probably reflects the relatively high proportion of zircon, in agreement with the elevated concentrations of Zr, Hf, U and Th (Table 2). The Light to Middle REE pattern of the Balagne albitite resembles that of SiO_2-rich plagiogranites from the Alpine Jurassic ophiolites (Borsi et al. 1996).

On the basis of the $\log(Fe_2O_3/K_2O)$ vs. $\log(SiO_2/Al_2O_3)$ scheme by Herron (1988) for the classification of terrigenic rocks, the selected quartzo-feldspathic sediments are arkoses. In particular, the specimen of quartzo-feldspathic breccia PC11 has lower SiO_2/Al_2O_3 ratios and higher Na_2O and K_2O concentrations than the quartzitic sandstone specimen PP1 (Table 2), in agreement with the lower modal quartz/feldspar ratio (see also Table 1). The CO_2 content of the quartzitic sandstone is 15 wt% and corresponds to a total modal amount of calcite of 35 mol%. The quartzo-feldspathic clastic sediments have nearly parallel REE patterns, characterized by a marked LREE enrichment and a slight HREE depletion relative to MREE, and a significant negative Eu anomaly (Fig. 4b). These patterns resemble the REE profile defined by the NASC (North American Shale Composite, Gromet et al. 1984). The quartzo-feldspathic breccia shows higher REE abundances than the quartzitic sandstone.

7 U–Pb zircon geochronology

7.1 The albitite from the intrusive sequence of the Moltifao tectonic slice

Twenty-eight zircon grains were separated from the albitite specimen GM1. They are 50–150 μm in size and mainly consist of pale pink fragments, typically irregularly fractured and in places showing crystal faces. The zircons have

Table 3 LA-ICP-MS U–Pb data of zircons from the albitite (sample GM1)

Identifier	Data for Tera-Wasserburg plot[a]				$^{208}Pb/^{206}Pb$	1 *s* %	Data for Wetherill plot[a]					$^{208}Pb/^{232}Th$
	$^{238}U/^{206}Pb$	1 *s* %	$^{207}Pb/^{206}Pb$	1 *s* %			$^{207}Pb/^{235}U$	1 *s* %	$^{206}Pb/^{238}U$	1 *s* %	Rho	
Z5	40.29	1.3	0.0571	4.80	#N/A	#N/A	0.1970	4.8	0.0248	1.3	0.27	#N/A
Z7	39.59	1.5	0.0515	5.30	#N/A	#N/A	0.1870	5.3	0.0253	1.5	0.28	#N/A
Z9	41.37	1.9	0.0602	7.30	#N/A	#N/A	0.1990	6.9	0.0242	1.9	0.27	#N/A
Z9b	42.07	1.6	0.0475	6.60	#N/A	#N/A	0.1560	6.1	0.0238	1.6	0.26	#N/A
Z12	42.79	1.5	0.0488	4.60	#N/A	#N/A	0.1610	4.6	0.0234	1.5	0.32	#N/A
Z12b	40.54	1.4	0.0485	4.90	#N/A	#N/A	0.1680	4.9	0.0247	1.4	0.28	#N/A
Z15	38.85	1.7	0.0586	6.10	#N/A	#N/A	0.2090	5.9	0.0257	1.7	0.29	#N/A
Z16	42.21	1.3	0.0522	5.00	#N/A	#N/A	0.1690	4.7	0.0237	1.3	0.28	#N/A
Z17	40.97	1.7	0.0530	6.80	#N/A	#N/A	0.1740	6.7	0.0244	1.7	0.25	#N/A
Z19	38.61	1.4	0.0562	4.70	#N/A	#N/A	0.1990	4.3	0.0259	1.4	0.32	#N/A
Z20	40.54	1.9	0.0607	7.40	#N/A	#N/A	0.2040	7.2	0.0247	1.9	0.26	#N/A
Z23	40.37	1.5	0.0506	7.00	#N/A	#N/A	0.1660	6.7	0.0248	1.5	0.23	#N/A
Z29	37.78	1.7	0.0645	6.90	#N/A	#N/A	0.2260	6.8	0.0265	1.7	0.26	#N/A
Z30	38.42	1.8	0.0574	5.90	#N/A	#N/A	0.1990	5.7	0.0260	1.8	0.31	#N/A
Z31	37.98	1.2	0.0521	4.60	#N/A	#N/A	0.1830	4.4	0.0263	1.2	0.27	#N/A
Z32	38.94	1.4	0.0526	4.90	#N/A	#N/A	0.1830	4.9	0.0257	1.4	0.28	#N/A
Z33	39.86	1.5	0.0510	6.40	#N/A	#N/A	0.1700	6.3	0.0251	1.5	0.25	#N/A
Z34	37.91	1.6	0.0660	5.80	#N/A	#N/A	0.2260	5.5	0.0264	1.6	0.29	#N/A
Z35	37.48	1.8	0.0594	8.00	#N/A	#N/A	0.2040	7.7	0.0267	1.8	0.23	#N/A
Z36	40.19	1.7	0.0532	5.50	#N/A	#N/A	0.1760	5.3	0.0249	1.7	0.32	#N/A
Z38	40.32	2.0	0.0641	8.00	#N/A	#N/A	0.2150	8.0	0.0248	2.0	0.26	#N/A
Z39	39.79	1.4	0.0559	5.20	#N/A	#N/A	0.1870	5.0	0.0251	1.4	0.28	#N/A
Z40	36.63	2.4	0.0610	11.70	#N/A	#N/A	0.2020	10.4	0.0273	2.4	0.23	#N/A
Z41	40.26	1.6	0.0534	6.10	#N/A	#N/A	0.1840	6.1	0.0248	1.6	0.26	#N/A
Z42	39.15	1.5	0.0600	9.40	#N/A	#N/A	0.2130	12.2	0.0255	1.5	0.12	#N/A
Z43	39.84	2.6	0.0540	15.00	#N/A	#N/A	0.1660	13.1	0.0251	2.6	0.20	#N/A
Z44	39.87	1.4	0.0507	5.80	#N/A	#N/A	0.1720	5.6	0.0251	1.4	0.25	#N/A
Z45	40.13	1.5	0.0655	4.90	#N/A	#N/A	0.2220	4.8	0.0249	1.5	0.30	#N/A
91500	5.55	1.4	0.0716	4.80	#N/A	#N/A	1.7300	4.3	0.1802	1.4	0.31	#N/A
91500	5.54	1.2	0.0767	4.40	#N/A	#N/A	1.8800	4.3	0.1804	1.2	0.28	#N/A

Table 3 continued

Identifier	1 *s* %	Dates[a]									$^{208}Pb/^{232}Th$	2*s* abs	$2s_{sys}$ abs	% Conc[b]
		$^{207}Pb/^{206}Pb$	2 *s* abs	2 s_{sys} abs	$^{206}Pb/^{238}U$	2 *s* abs	2 s_{sys} abs	$^{207}Pb/^{235}U$	2*s* abs	$2s_{sys}$ abs				
Z5	#N/A	495	43	48	158	4	4	183	16	18	#N/A	#N/A	#N/A	13
Z7	#N/A	263	26	28	161	5	5	174	17	18	#N/A	#N/A	#N/A	8
Z9	#N/A	611	85	89	154	6	6	184	24	25	#N/A	#N/A	#N/A	16
Z9b	#N/A	74	9	10	151	5	5	147	17	18	#N/A	#N/A	#N/A	3
Z12	#N/A	138	11	13	149	4	4	152	12	14	#N/A	#N/A	#N/A	2
Z12b	#N/A	124	11	12	157	4	4	158	14	16	#N/A	#N/A	#N/A	0
Z15	#N/A	552	63	67	164	5	6	193	21	23	#N/A	#N/A	#N/A	15
Z16	#N/A	294	27	30	151	4	4	159	13	15	#N/A	#N/A	#N/A	5
Z17	#N/A	329	43	45	155	5	5	163	21	22	#N/A	#N/A	#N/A	5
Z19	#N/A	460	38	43	165	4	5	184	14	16	#N/A	#N/A	#N/A	11
Z20	#N/A	629	90	94	157	6	6	189	26	27	#N/A	#N/A	#N/A	17
Z23	#N/A	223	30	31	158	5	5	156	20	21	#N/A	#N/A	#N/A	1
Z29	#N/A	758	100	105	168	6	6	207	27	28	#N/A	#N/A	#N/A	19
Z30	#N/A	507	56	59	166	6	6	184	19	21	#N/A	#N/A	#N/A	10
Z31	#N/A	290	24	27	168	4	4	171	13	15	#N/A	#N/A	#N/A	2
Z32	#N/A	312	28	31	163	4	4	171	15	17	#N/A	#N/A	#N/A	4
Z33	#N/A	241	29	31	160	5	5	159	19	20	#N/A	#N/A	#N/A	0
Z34	#N/A	806	87	93	168	5	5	207	21	23	#N/A	#N/A	#N/A	19
Z35	#N/A	582	90	93	170	6	6	189	28	29	#N/A	#N/A	#N/A	10
Z36	#N/A	337	34	37	158	5	5	165	16	17	#N/A	#N/A	#N/A	4
Z38	#N/A	745	115	119	158	6	6	198	30	31	#N/A	#N/A	#N/A	20
Z39	#N/A	448	43	47	160	4	4	174	16	17	#N/A	#N/A	#N/A	8
Z40	#N/A	639	147	149	174	8	8	187	38	39	#N/A	#N/A	#N/A	7
Z41	#N/A	346	40	42	158	5	5	171	20	21	#N/A	#N/A	#N/A	8
Z42	#N/A	604	111	113	163	5	5	196	47	48	#N/A	#N/A	#N/A	17
Z43	#N/A	371	110	111	160	8	8	156	40	41	#N/A	#N/A	#N/A	2
Z44	#N/A	227	25	26	160	4	4	161	17	18	#N/A	#N/A	#N/A	1
Z45	#N/A	790	70	77	159	4	5	204	17	19	#N/A	#N/A	#N/A	22
91500	#N/A	975	86	94	1068	28	28	1020	77	88	#N/A	#N/A	#N/A	5
91500	#N/A	1113	86	97	1069	24	26	1074	80	92	#N/A	#N/A	#N/A	0

Uncertainties quoted without components related to systematic error unless otherwise stated

#N/A not available

[a] Data not corrected for common-Pb

[b] Discordance (absolute value of the differences between $^{206}Pb/^{238}U$ and $^{207}Pb/^{235}U$ dates) = $[1-(^{206}Pb/^{238}U/^{207}Pb/^{235}U)] \times 100$

Table 4 LA-ICP-MS U–Pb data of zircons from the quartz-feldspathic breccia (sample PC11)

Identifier	Data for Tera-Wasserburg plot[a]				$^{208}Pb/^{206}Pb$	1 *s*%	Data for Wetherill plot[a]					$^{208}Pb/^{232}Th$
	$^{238}U/^{206}Pb$	1 *s*%	$^{207}Pb/^{206}Pb$	1 *s*%			$^{207}Pb/^{235}U$	1 *s*%	$^{206}Pb/^{238}U$	1 *s*%	Rho	
Z1	22.47	3.0	0.0568	5.4	#N/A	#N/A	0.3560	6.0	0.0445	3.0	0.18	#N/A
Z2	20.96	2.8	0.0540	3.5	#N/A	#N/A	0.3530	4.4	0.0477	2.8	0.08	#N/A
Z3	20.99	2.7	0.0500	2.5	#N/A	#N/A	0.3270	3.7	0.0476	2.7	0.10	#N/A
Z7	23.07	2.8	0.0536	2.1	#N/A	#N/A	0.3130	3.4	0.0433	2.8	0.16	#N/A
Z8	28.01	2.8	0.0502	2.8	#N/A	#N/A	0.2030	3.7	0.0357	2.8	0.09	#N/A
Z9	27.01	2.7	0.0509	2.8	#N/A	#N/A	0.2160	3.9	0.0370	2.7	0.05	#N/A
Z12	23.15	2.8	0.0501	2.8	#N/A	#N/A	0.3050	3.8	0.0432	2.8	0.18	#N/A
Z13	24.17	2.8	0.0507	3.9	#N/A	#N/A	0.2390	4.6	0.0414	2.8	0.00	#N/A
Z14	23.33	2.7	0.0497	2.5	#N/A	#N/A	0.3060	3.8	0.0429	2.7	0.22	#N/A
Z15	28.00	2.8	0.0508	1.7	#N/A	#N/A	0.2080	3.1	0.0357	2.8	0.18	#N/A
Z17	23.26	2.8	0.0508	3.0	#N/A	#N/A	0.3010	3.8	0.0430	2.8	0.10	#N/A
Z18	22.65	2.7	0.0522	2.9	#N/A	#N/A	0.3160	3.8	0.0442	2.7	0.03	#N/A
Z19	22.67	2.7	0.0505	2.1	#N/A	#N/A	0.3070	3.3	0.0441	2.7	0.16	#N/A
Z20	22.56	2.7	0.0524	3.0	#N/A	#N/A	0.3220	3.9	0.0443	2.7	0.02	#N/A
Z21	22.90	2.7	0.0519	2.6	#N/A	#N/A	0.3130	3.7	0.0437	2.7	0.17	#N/A
Z22	22.92	2.8	0.0514	2.5	#N/A	#N/A	0.3100	3.7	0.0436	2.8	0.06	#N/A
Z23	22.06	2.8	0.0496	2.7	#N/A	#N/A	0.3220	3.7	0.0453	2.8	0.07	#N/A
Z24	23.40	2.8	0.0490	3.4	#N/A	#N/A	0.2930	4.3	0.0427	2.8	0.15	#N/A
Z25	22.11	2.8	0.0499	2.1	#N/A	#N/A	0.3180	3.3	0.0452	2.8	0.15	#N/A
Z26	21.65	2.8	0.0513	2.9	#N/A	#N/A	0.3240	3.9	0.0462	2.8	0.12	#N/A
Z27	21.60	2.8	0.0515	4.0	#N/A	#N/A	0.3290	4.9	0.0463	2.8	0.10	#N/A
Z28	21.75	2.7	0.0507	2.9	#N/A	#N/A	0.3240	3.9	0.0460	2.7	0.12	#N/A
Z30	22.33	2.8	0.0511	3.2	#N/A	#N/A	0.3190	4.1	0.0448	2.8	0.01	#N/A
Z32	22.30	2.7	0.0515	2.4	#N/A	#N/A	0.3220	3.6	0.0449	2.7	0.09	#N/A
Z34	22.27	2.7	0.0501	2.1	#N/A	#N/A	0.3100	3.4	0.0449	2.7	0.13	#N/A
Z35	21.94	2.6	0.0516	1.6	#N/A	#N/A	0.3287	3.0	0.0456	2.6	0.09	#N/A
Z36	25.81	2.7	0.0509	2.3	#N/A	#N/A	0.2257	3.3	0.0388	2.7	0.16	#N/A
Z38	22.83	2.7	0.0507	2.3	#N/A	#N/A	0.3060	3.4	0.0438	2.7	0.15	#N/A
Z40	25.25	2.8	0.0493	2.2	#N/A	#N/A	0.2223	3.4	0.0396	2.8	0.19	#N/A
Z41	21.62	2.8	0.0522	3.4	#N/A	#N/A	0.3360	4.2	0.0463	2.8	0.06	#N/A

Table 4 continued

Identifier	Data for Tera-Wasserburg plot[a]				$^{208}Pb/^{206}Pb$	1 *s*%	Data for Wetherill plot[a]					$^{208}Pb/^{232}Th$
	$^{238}U/^{206}Pb$	1 *s*%	$^{207}Pb/^{206}Pb$	1 *s*%			$^{207}Pb/^{235}U$	1 *s*%	$^{206}Pb/^{238}U$	1 *s*%	Rho	
Z42	23.20	3.1	0.0569	5.3	#N/A	#N/A	0.3430	6.0	0.0431	3.1	0.15	#N/A
Z43	26.23	2.8	0.0512	3.5	#N/A	#N/A	0.2240	4.5	0.0381	2.8	0.14	#N/A
Z44	24.18	2.8	0.0655	3.0	#N/A	#N/A	0.3830	3.8	0.0414	2.8	0.01	#N/A
Z45	23.95	2.8	0.0538	4.0	#N/A	#N/A	0.2570	4.7	0.0418	2.8	0.01	#N/A
Z47	22.58	2.7	0.0487	2.1	#N/A	#N/A	0.2980	3.4	0.0443	2.7	0.18	#N/A
Z48	26.41	2.8	0.0494	3.1	#N/A	#N/A	0.2150	4.0	0.0379	2.8	0.07	#N/A
Z49	22.69	2.7	0.0478	3.5	#N/A	#N/A	0.2870	4.2	0.0441	2.7	0.02	#N/A

Identifier	1 *s*%	Dates[a]									$^{208}Pb/^{232}Th$	2*s* abs	$2s_{sys}$ abs	% Conc[b]
		$^{207}Pb/^{206}Pb$	2 *s* abs	2 s_{sys} ab	$^{206}Pb/^{238}U$	2 *s* abs	2 s_{sys} ab	$^{207}Pb/^{235}U$	2*s* abs	2s_{sys} ab				
Z1	#N/A	300	190	190	281	9	17	286	27	30	#N/A	#N/A	#N/A	2%
Z2	#N/A	270	120	120	301	7	17	298	18	23	#N/A	#N/A	#N/A	1%
Z3	#N/A	218	97	97	300	5	16	289	13	18	#N/A	#N/A	#N/A	4%
Z7	#N/A	318	83	83	273	5	15	274	10	16	#N/A	#N/A	#N/A	0%
Z8	#N/A	190	100	100	226	5	12	188	9	13	#N/A	#N/A	#N/A	20%
Z9	#N/A	200	100	100	234	4	12	198	10	14	#N/A	#N/A	#N/A	18%
Z12	#N/A	190	110	110	272	6	15	268	13	18	#N/A	#N/A	#N/A	2%
Z13	#N/A	170	140	140	261	6	14	212	15	18	#N/A	#N/A	#N/A	23%
Z14	#N/A	184	96	96	271	5	14	268	12	18	#N/A	#N/A	#N/A	1%
Z15	#N/A	244	70	70	227	4	12	192	6	11	#N/A	#N/A	#N/A	18%
Z17	#N/A	200	110	110	271	5	15	265	13	18	#N/A	#N/A	#N/A	3%
Z18	#N/A	240	110	110	278	5	15	278	13	18	#N/A	#N/A	#N/A	0%
Z19	#N/A	204	80	80	279	5	15	275	9	15	#N/A	#N/A	#N/A	1%
Z20	#N/A	240	110	110	279	6	15	279	14	19	#N/A	#N/A	#N/A	0%
Z21	#N/A	284	97	97	275	5	15	274	12	18	#N/A	#N/A	#N/A	0%
Z22	#N/A	229	95	95	275	5	15	275	12	17	#N/A	#N/A	#N/A	0%
Z23	#N/A	200	100	100	286	5	15	282	13	19	#N/A	#N/A	#N/A	1%
Z24	#N/A	190	120	120	270	6	15	259	16	20	#N/A	#N/A	#N/A	4%
Z25	#N/A	219	78	78	285	5	15	280	10	16	#N/A	#N/A	#N/A	2%
Z26	#N/A	260	110	110	291	6	16	288	14	19	#N/A	#N/A	#N/A	1%
Z27	#N/A	190	140	140	292	6	16	282	20	24	#N/A	#N/A	#N/A	3%
Z28	#N/A	230	110	110	290	5	15	284	14	19	#N/A	#N/A	#N/A	2%
Z30	#N/A	260	120	120	283	6	15	280	15	20	#N/A	#N/A	#N/A	1%
Z32	#N/A	268	92	92	283	5	15	284	12	18	#N/A	#N/A	#N/A	0%

Table 4 continued

Identifier	1 *s*%	Dates[a]									$^{208}Pb/^{232}Th$	2*s* abs	$2s_{sys}$ abs	% Conc[b]
		$^{207}Pb/^{206}Pb$	2 *s* abs	2 s_{sys} ab	$^{206}Pb/^{238}U$	2 *s* abs	2 s_{sys} ab	$^{207}Pb/^{235}U$	2*s* abs	$2s_{sys}$ ab				
Z34	#N/A	174	78	78	283	4	15	274	9	16	#N/A	#N/A	#N/A	3%
Z35	#N/A	247	67	67	288	5	15	287	7	15	#N/A	#N/A	#N/A	0%
Z36	#N/A	209	83	83	245	4	13	206	8	13	#N/A	#N/A	#N/A	19%
Z38	#N/A	214	86	86	276	4	15	275	10	16	#N/A	#N/A	#N/A	0%
Z40	#N/A	198	85	85	250	5	14	204	8	13	#N/A	#N/A	#N/A	23%
Z41	#N/A	240	120	120	291	6	16	289	16	21	#N/A	#N/A	#N/A	1%
Z42	#N/A	410	200	200	272	10	17	301	28	31	#N/A	#N/A	#N/A	10%
Z43	#N/A	220	130	130	241	5	13	203	13	17	#N/A	#N/A	#N/A	19%
Z44	#N/A	710	120	120	261	6	14	326	15	21	#N/A	#N/A	#N/A	20%
Z45	#N/A	260	150	150	265	6	14	226	16	19	#N/A	#N/A	#N/A	17%
Z47	#N/A	155	79	79	279	5	15	263	9	15	#N/A	#N/A	#N/A	6%
Z48	#N/A	180	110	110	240	5	13	197	11	14	#N/A	#N/A	#N/A	22%
Z49	#N/A	60	120	120	278	5	15	252	15	19	#N/A	#N/A	#N/A	10%

Uncertainties quoted without components related to systematic error unless otherwise stated

N/A not available

[a] Data not corrected for common-Pb

[b] Discordance (absolute value of the differences between $^{206}Pb/^{238}U$ and $^{207}Pb/^{235}U$ dates) = $[1-(^{206}Pb/^{238}U/^{207}Pb/^{235}U)] \times 100$

Table 5 LA-ICP-MS U–Pb data of zircons from the quartzitic sandstone (sample PP1)

Identifier	Data for Tera-Wasserburg plot[a]				$^{208}Pb/^{206}Pb$	1 *s*%	Data for Wetherill plot[a]					$^{208}Pb/^{232}Th$
	$^{238}U/^{206}Pb$	1 *s*%	$^{207}Pb/^{206}Pb$	1 *s*%			$^{207}Pb/^{235}U$	1 *s*%	$^{206}Pb/^{238}U$	1 *s*%	Rho	
Z1	13.55	1.9	0.0553	4.4	#N/A	#N/A	0.5560	3.9	0.0738	1.9	0.15	#N/A
Z2	22.01	1.9	0.0534	5.1	#N/A	#N/A	0.3310	4.5	0.0454	1.9	0.07	#N/A
Z4(a)	21.82	1.9	0.0524	4.5	#N/A	#N/A	0.3320	3.8	0.0458	1.9	0.11	#N/A
Z4(b)	22.86	1.8	0.0553	4.5	#N/A	#N/A	0.3380	4.0	0.0437	1.8	0.11	#N/A
Z6	23.82	1.8	0.0550	4.3	#N/A	#N/A	0.3220	3.7	0.0420	1.8	0.25	#N/A
Z8	20.33	1.8	0.0527	4.4	#N/A	#N/A	0.3630	3.7	0.0492	1.8	0.14	#N/A
Z10	22.86	1.8	0.0511	4.3	#N/A	#N/A	0.3080	3.7	0.0438	1.8	0.23	#N/A
Z11	24.02	1.8	0.0528	4.2	#N/A	#N/A	0.3049	3.6	0.0416	1.8	0.21	#N/A
Z12	20.53	2.0	0.0547	5.1	#N/A	#N/A	0.3630	4.5	0.0487	2.0	0.05	#N/A
Z13	23.93	1.9	0.0510	4.6	#N/A	#N/A	0.2960	4.1	0.0418	1.9	0.27	#N/A
Z14	26.35	1.8	0.0628	4.2	#N/A	#N/A	0.3290	3.6	0.0380	1.8	0.17	#N/A
Z15core	29.57	1.9	0.0536	4.3	#N/A	#N/A	0.2529	3.8	0.0338	1.9	0.23	#N/A
Z15rim	22.37	1.9	0.0581	5.1	#N/A	#N/A	0.3530	4.7	0.0447	1.9	0.24	#N/A
Z16	26.96	1.8	0.0570	4.2	#N/A	#N/A	0.2990	3.7	0.0371	1.8	0.20	#N/A
Z17	24.20	1.8	0.0588	4.5	#N/A	#N/A	0.3320	3.9	0.0413	1.8	0.19	#N/A
Z18	29.59	1.8	0.0629	4.4	#N/A	#N/A	0.2960	3.7	0.0338	1.8	0.13	#N/A
Z20	25.08	1.9	0.0555	4.5	#N/A	#N/A	0.3120	3.8	0.0399	1.9	0.09	#N/A
Z22	22.96	1.8	0.0507	4.7	#N/A	#N/A	0.3100	4.4	0.0436	1.8	0.20	#N/A
Z25	23.20	1.9	0.0544	4.5	#N/A	#N/A	0.3310	3.9	0.0431	1.9	0.06	#N/A
Z26	22.08	1.9	0.0520	4.6	#N/A	#N/A	0.3300	4.1	0.0453	1.9	0.07	#N/A
Z27	23.13	1.9	0.0524	4.7	#N/A	#N/A	0.3120	4.0	0.0432	1.9	0.07	#N/A
Z29	23.00	1.7	0.0514	4.4	#N/A	#N/A	0.3090	3.9	0.0435	1.7	0.11	#N/A
Z30	25.35	1.9	0.0535	4.3	#N/A	#N/A	0.2920	3.8	0.0395	1.9	0.25	#N/A
Z31	22.82	1.8	0.0519	4.5	#N/A	#N/A	0.3140	4.0	0.0438	1.8	0.08	#N/A
Z32	23.79	1.8	0.0512	4.4	#N/A	#N/A	0.2930	3.9	0.0420	1.8	0.16	#N/A
Z33	22.79	1.8	0.0527	4.5	#N/A	#N/A	0.3190	3.9	0.0439	1.8	0.09	#N/A
Z35	22.65	1.8	0.0525	5.0	#N/A	#N/A	0.3170	4.4	0.0442	1.8	0.08	#N/A
Z35b	27.59	1.8	0.0520	4.7	#N/A	#N/A	0.2380	4.2	0.0363	1.8	0.07	#N/A
Z36	22.72	1.9	0.0543	4.4	#N/A	#N/A	0.3420	3.9	0.0440	1.9	0.28	#N/A
Z37	28.80	1.7	0.0578	4.3	#N/A	#N/A	0.2502	3.8	0.0347	1.7	0.18	#N/A
Z40	33.11	2.6	0.1071	4.7	#N/A	#N/A	0.4180	3.7	0.0302	2.6	0.13	#N/A
Z41	22.74	1.8	0.0530	4.5	#N/A	#N/A	0.3140	4.0	0.0440	1.8	0.12	#N/A
Z43	23.87	1.9	0.0563	4.5	#N/A	#N/A	0.3220	4.0	0.0419	1.9	0.16	#N/A
Z44	27.40	1.9	0.0576	4.3	#N/A	#N/A	0.2830	3.9	0.0365	1.9	0.26	#N/A
Z45	24.19	1.8	0.0517	4.4	#N/A	#N/A	0.2950	3.7	0.0413	1.8	0.08	#N/A

Table 5 continued

Identifier	Data for Tera-Wasserburg plot[a]				$^{208}Pb/^{206}Pb$	1 *s*%	Data for Wetherill plot[a]					$^{208}Pb/^{232}Th$
	$^{238}U/^{206}Pb$	1 *s*%	$^{207}Pb/^{206}Pb$	1 *s*%			$^{207}Pb/^{235}U$	1 *s*%	$^{206}Pb/^{238}U$	1 *s*%	Rho	
Z48	23.21	1.7	0.0517	4.4	#N/A	#N/A	0.3070	3.9	0.0431	1.7	0.09	#N/A
Z51	22.17	1.9	0.0531	4.6	#N/A	#N/A	0.3270	4.1	0.0451	1.9	0.14	#N/A
Z53	30.31	2.0	0.0541	4.3	#N/A	#N/A	0.2410	3.9	0.0330	2.0	0.45	#N/A

Identifier	1 *s*%	Dates[a]									$^{208}Pb/^{232}Th$	2*s* abs3	$2s_{sys}$ abs	% Conc[b]
		$^{207}Pb/^{206}Pb$	2 *s* abs	2 s_{sys} abs	$^{206}Pb/^{238}U$	2 *s* abs	2 s_{sys} abs	$^{207}Pb/^{235}U$	2*s* abs	$2s_{sys}$ abs				
Z1	#N/A	383	90	180	459	9	17	445	15	27	#N/A	#N/A	#N/A	3%
Z2	#N/A	240	120	180	286	6	10	286	16	23	#N/A	#N/A	#N/A	0%
Z4(a)	#N/A	288	89	170	289	5	10	291	11	19	#N/A	#N/A	#N/A	1%
Z4(b)	#N/A	364	92	170	276	5	10	294	12	20	#N/A	#N/A	#N/A	6%
Z6	#N/A	377	76	180	265	5	10	282	9	18	#N/A	#N/A	#N/A	6%
Z8	#N/A	303	79	170	309	6	11	313	10	20	#N/A	#N/A	#N/A	1%
Z10	#N/A	220	75	170	276	5	10	273	9	18	#N/A	#N/A	#N/A	1%
Z11	#N/A	292	64	160	263	4	9	268	7	17	#N/A	#N/A	#N/A	2%
Z12	#N/A	360	120	190	306	7	11	317	17	24	#N/A	#N/A	#N/A	3%
Z13	#N/A	230	97	180	264	5	10	261	12	19	#N/A	#N/A	#N/A	1%
Z14	#N/A	650	76	180	240	4	9	287	9	18	#N/A	#N/A	#N/A	16%
Z15core	#N/A	328	77	170	214	4	8	228	8	15	#N/A	#N/A	#N/A	6%
Z15rim	#N/A	450	120	190	282	6	11	297	18	24	#N/A	#N/A	#N/A	5%
Z16	#N/A	464	76	170	235	4	8	265	8	17	#N/A	#N/A	#N/A	12%
Z17	#N/A	472	93	170	261	5	9	287	12	20	#N/A	#N/A	#N/A	9%
Z18	#N/A	669	84	180	214	4	8	264	9	17	#N/A	#N/A	#N/A	19%
Z20	#N/A	401	95	180	252	6	10	276	11	19	#N/A	#N/A	#N/A	9%
Z22	#N/A	190	100	170	275	5	10	272	14	21	#N/A	#N/A	#N/A	1%
Z25	#N/A	367	97	180	272	5	10	288	12	20	#N/A	#N/A	#N/A	5%
Z26	#N/A	259	98	180	286	5	10	288	12	20	#N/A	#N/A	#N/A	1%
Z27	#N/A	284	99	170	273	5	10	274	12	19	#N/A	#N/A	#N/A	0%
Z29	#N/A	253	83	170	274	4	9	271	10	18	#N/A	#N/A	#N/A	1%
Z30	#N/A	317	81	170	249	5	9	259	9	18	#N/A	#N/A	#N/A	4%
Z31	#N/A	304	91	170	276	5	10	277	11	19	#N/A	#N/A	#N/A	0%
Z32	#N/A	254	84	170	266	4	9	261	10	18	#N/A	#N/A	#N/A	2%
Z33	#N/A	284	91	180	277	5	10	279	11	19	#N/A	#N/A	#N/A	1%
Z35	#N/A	300	110	180	278	5	10	280	14	21	#N/A	#N/A	#N/A	1%
Z35b	#N/A	230	110	180	230	4	8	214	11	17	#N/A	#N/A	#N/A	7%

Table 5 continued

Identifier	1 *s*%	Dates[a]									$^{208}Pb/^{232}Th$	2*s* abs3	$2s_{sys}$ abs	% Conc[b]
		$^{207}Pb/^{206}Pb$	2 *s* abs	2 s_{sys} abs	$^{206}Pb/^{238}U$	2 *s* abs	2 s_{sys} abs	$^{207}Pb/^{235}U$	2*s* abs	$2s_{sys}$ abs				
Z36	#N/A	357	85	170	278	6	10	297	12	20	#N/A	#N/A	#N/A	7%
Z37	#N/A	446	82	170	220	4	8	225	8	15	#N/A	#N/A	#N/A	3%
Z40	#N/A	1680	110	190	192	8	10	354	11	22	#N/A	#N/A	#N/A	46%
Z41	#N/A	291	91	170	277	5	10	279	11	19	#N/A	#N/A	#N/A	1%
Z43	#N/A	430	98	180	265	6	10	287	12	20	#N/A	#N/A	#N/A	8%
Z44	#N/A	476	80	170	231	5	9	251	9	17	#N/A	#N/A	#N/A	8%
Z45	#N/A	284	83	170	262	4	9	262	9	18	#N/A	#N/A	#N/A	0%
Z48	#N/A	255	85	170	272	4	10	271	10	19	#N/A	#N/A	#N/A	0%
Z51	#N/A	270	100	180	285	5	10	284	13	20	#N/A	#N/A	#N/A	0%
Z53	#N/A	336	82	170	209	5	8	218	9	15	#N/A	#N/A	#N/A	4%

Uncertainties quoted without components related to systematic error unless otherwise stated

N/A not available

[a] Data not corrected for common-Pb

[b] Discordance (absolute value of the differences between $^{206}Pb/^{238}U$ and $^{207}Pb/^{235}U$ dates) = $[1-(^{206}Pb/^{238}U/^{207}Pb/^{235}U)] \times 100$

Table 6 Data reporting template (information) for LA-ICP-MS U-Th–Pb data

Laboratory and sample preparation	
Laboratory name	C.N.R.–Istituto di Geoscienze e Georisorse, Unità di Pavia
Sample type/mineral	Detrital and magmatic zircons
Sample preparation	Conventional mineral separation, 1 inch resin mount, 1 μm polish to finish
Imaging	Cathodoluminescence
Laser ablation system	
Make, model and type	Geolas200Q-Microlas
Ablation cell and volume	95 cm^3
Laser wavelength (nm)	193 nm
Pulse width (ns)	20 ns
Fluence ($J.cm^{-2}$)	12 $J.cm^{-2}$
Repetition rate (Hz)	5 Hz
Ablation duration (secs)	Up to 60 s
Ablation pit depth/ablation rate	Not determined
Spot diameter (μm) nominal/actual	20 μm
Sampling mode/pattern	Static spot ablation
Carrier gas	100% He in the cell, Ar make-up gas combined using a Y-piece 50% along the sample transport line to the torch
Cell carrier gas flow (l/min)	0.7 l/min
ICP-MS instrument	
Make, model and type	HR-ICP-MS ELEMENT I ThermoFinnigan
Sample introduction	Ablation aerosol
RF power (W)	1200 W
Make-up gas flow (l/min)	0.7 l/min
Detection system	Secondary electron multiplier
Masses measured	202, 204, 206, 207, 208, 232, 238
Integration time per peak/dwell times (ms)	1.5 ms for Hg^{202}, Pb^{204}, Pb^{206}, Pb^{207}, Pb^{208}; 3.0 ms for U^{238} and Th^{232}
Total integration time per output datapoint (secs)	~1.2 s 120 s
'Sensitivity' as useful yield (%, element)	6×10^6 (%Th) [NIST610]
Dead time (ns)	25 ns
Data processing	
Gas blank	60 s of gas blank acquisition prior ablation
Calibration strategy	Zircon GJ1 used as primary external standard, zircon 91500 used as validation standard
Reference material info	GJ1 (Jackson et al. 2004) 91500 (Wiedenbeck et al. 1995)
Data processing package used/correction for LIEF	Iolite (Paton et al. 2010, 2011???) LIEF correction assumes reference material and samples behave identically
Mass discrimination	$^{207}Pb/^{206}Pb$ and $^{206}Pb/^{238}U$ normalised to reference material
Common-Pb correction, composition and uncertainty	No common-Pb correction applied to the data
Uncertainty level and propagation	Ages are quoted at 2 *s* absolute; propagation is by quadratic addition. Reproducibility and age uncertainty of reference material are propagated where appropriate
Quality control/validation	91500 (1065 Ma, Wiedenbeck et al. 1995)

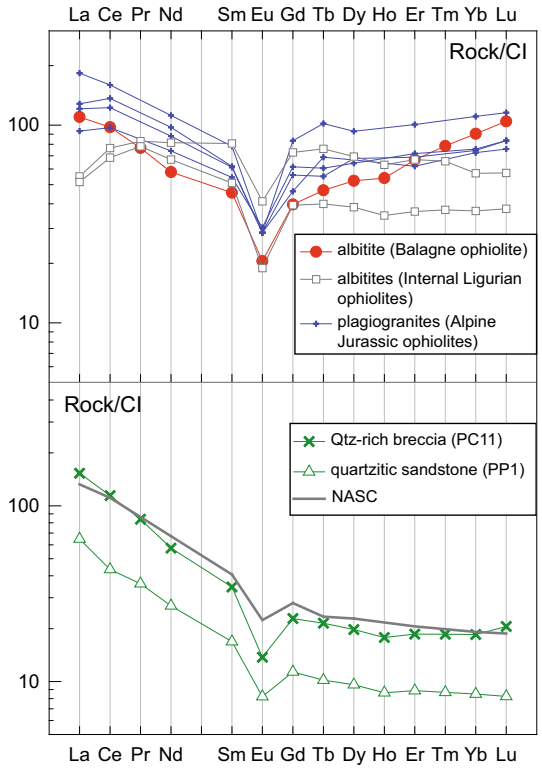

Fig. 4 Whole-rock REE compositions of the selected albitite and quartz-feldspathic clastic sediments normalized to CI chondrite (Anders and Ebihara 1982). The compositions of albitites from Internal Ligurian ophiolites (Tribuzio et al. 2014), SiO_2–rich plagiogranites (Borsi et al. 1996) and NASC (North American Shale Composite, Gromet et al. 1984) are reported for comparative purposes

low CL emission and commonly a faint oscillatory zoning with low contrast (Fig. 5a). Rare grains with an oscillatory zoning consisting of broad bands were also found. Turbid domains, showing pores and mineral inclusions are locally present (Fig. 5b) and resemble the spongy structure observed in zircons from modern spreading ridges (e.g., Grimes et al. 2009; Schwartz et al. 2010). This structure was interpreted to reflect alteration of original magmatic zircons by a fluid-driven reaction of dissolution and re-

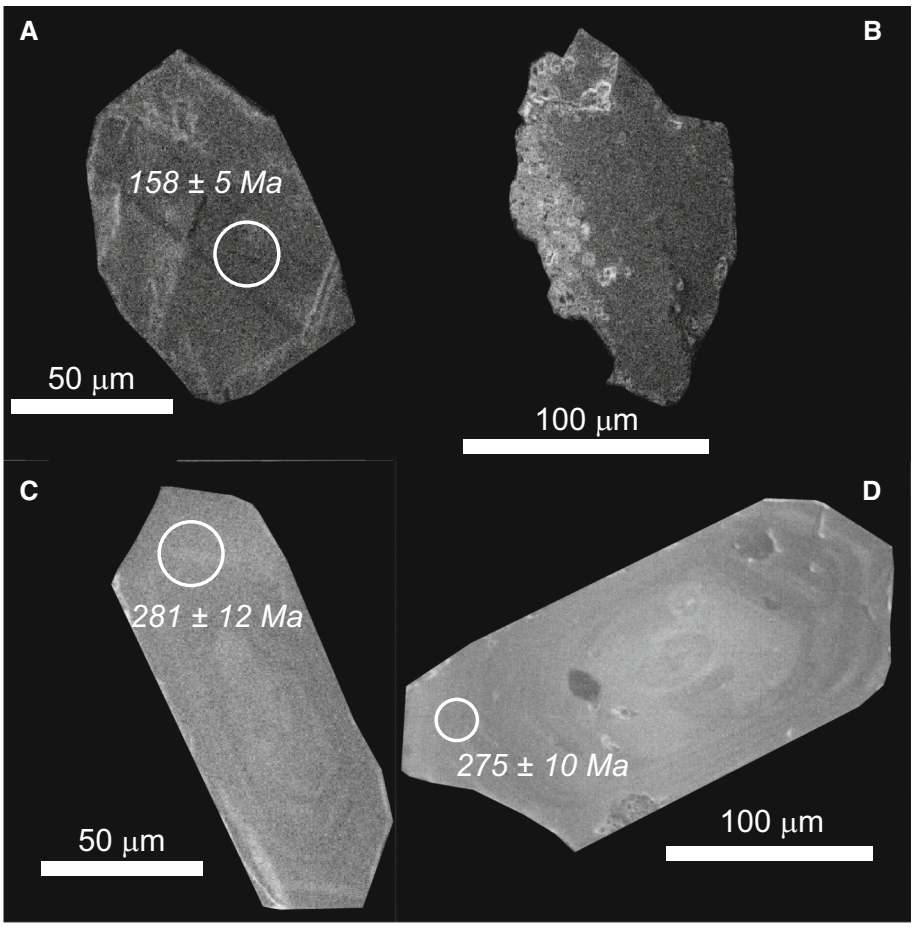

Fig. 5 Representative cathodoluminescence images of zircons with location of geochronological analyses. The ages shown in *italic* character are concordant ages (errors are 2). **a** zircon with a faint oscillatory zoning showing a broad low-cathodoluminescent core surrounded by a small, fine oscillatory zoned rim (albitite GM1). **b** zircon fragment showing *dark* un-zoned core and spongy structures on the rim (albitite GM1). **c** prismatic, oscillatory zoned zircon characterized by faint banding (quartz-feldspathic breccia PC11). **d** sub-prismatic zircon showing an inherited rounded core surrounded by a weakly luminescent oscillatory zoned rim (quartzitic sandstone PP1)

precipitation (see also Grimes et al. 2011). No inherited zircon domains were observed.

U–Pb zircon geochronology was carried out on zircon domains as free of fractures, pores and mineral inclusions as possible. Eighteen analyses yielded concordant $^{206}Pb/^{238}U$ and $^{207}Pb/^{235}U$ dates scattering from 174 ± 8 to 149 ± 4 Ma (2σ, Table 3). The 18 concordant dates yielded a weighted mean age of 159.0 ± 3.0 Ma (95% confidence level, MSWD = 6.3, Fig. 6a). The relatively high MSWD could be influenced by zircon domains that were either damaged by U-decay, affected by radiogenic Pb loss, or where common Pb was potentially stored (von Quadt et al. 2014). The remaining 10 zircon analyses were discordant with $^{206}Pb/^{238}U$ dates ranging from 168 ± 6 to 154 ± 6 Ma (2σ, Table 3). The discordance could reflect some radiogenic Pb loss; in addition, the discordant zircons most likely experienced common Pb contamination. A regression line calculation of data on a Tera-Wasserburg concordia diagram may be used to correct for common Pb contribution (Schoene 2014). On this diagram (Fig. 6), we obtained a lower intercept age of 158.1 ± 3.2 Ma (95% confidence level, MSWD = 2.1, N = 28) considering all concordant and discordant data.

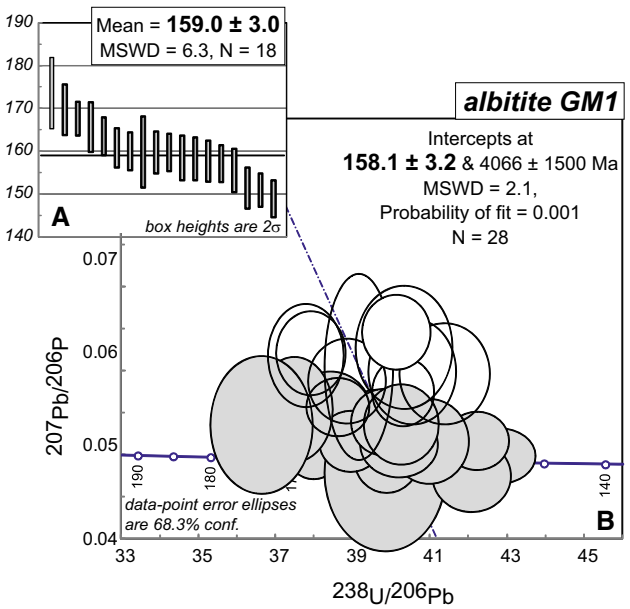

Fig. 6 **a** Weighted average plot of concordant zircon analyses from the albitite GM1. **b** Tera-Wasserburg U–Pb concordia diagram of concordant (*grey* ellipses) and discordant (*empty* ellipses) zircon analyses from albitite GM1

This lower intercept age is within error the weighted mean age given by the concordant dates. Although the high MSWD associated with the weighted mean age left some uncertainty, we propose that the albitite GM1 crystallized at 159.0 ± 3.0. This statement implies that the event of common Pb contamination was nearly coeval with the crystallization of the albitite.

7.2 The quartzo-feldspathic breccia from the basalt-sedimentary succession

156 zircon grains were separated from the quartzo-feldspathic breccia PC11. They are dominated by a population of colorless transparent crystals; about 15% of separated zircons are opaque. The zircons are mainly prismatic; sub-prismatic to stubby grains are also present. The zircon length/width aspect ratio varies between 1 and 0.3. No systematic differences in shape and CL inner structure were found between the transparent and opaque zircon populations. CL imaging typically shows inner structure with oscillatory zoning (Fig. 5c), which is locally characterized by faintly to broad banding. Rare not zoned domains and/or inherited cores are also present.

Thirty-seven grains of zircon were dated by LA-ICPMS. Twenty-seven analyses resulted in concordant $^{206}Pb/^{238}U$ and $^{207}Pb/^{235}U$ dates (Table 4), which yielded a mean concordia age of 280.0 ± 2.4 (2σ, MSWD = 1.9, Fig. 7a). The remaining 10 analyses are discordant and did not furnish considerable geochronological information (Table 4).

7.3 The quartzitic sandstone from the basalt-sedimentary succession

Zircons separated from the quartzitic sandstone PP1 (146 grains) consist of pink transparent to dark pink opaque grains. They are mainly stubby, sub-prismatic to prismatic and sharp and have aspect ratio (length/width) between 1 and 0.3. Rounded grains are rare. The zircons have low CL emission and are not zoned, or only exhibit a weak oscillatory zoning (Fig. 5d). Dark cores and faintly broad zoned domains were locally found.

Thirty-eight grains were dated. Thirty-four analyses yielded concordant $^{206}Pb/^{238}U$ and $^{207}Pb/^{235}U$ dates (Table 5) that range from ~460 to ~210 Ma. When plotted on the age probability distribution diagram (Fig. 7b), 17 of the concordant U–Pb dates identify a main peak at 278.8 ± 2.3 Ma (2σ, MSWD = 1.3, weighted average age). Three older concordant $^{206}Pb/^{238}U$ and $^{207}Pb/^{235}U$ dates at 457 ± 15 Ma (2σ, $N = 1$) and 309 ± 7 Ma (2σ, weighted average age, $N = 2$) were also found. The remaining fourteen concordant U–Pb dates fall in two slightly younger age clusters at 262.2 ± 5.9 Ma (2σ, concordia age, MSWD = 2.3, $N = 9$) and

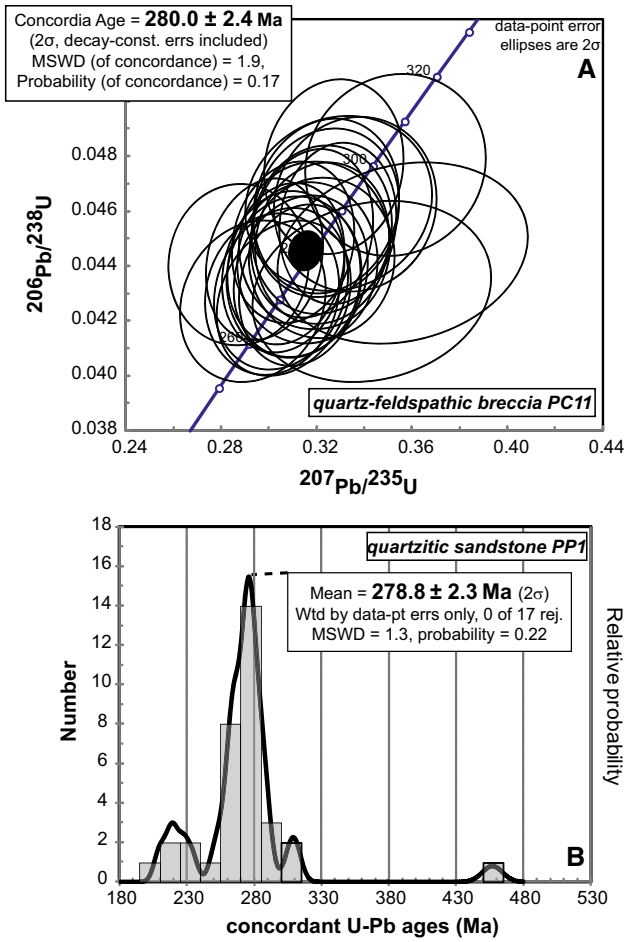

Fig. 7 **a** U–Pb Concordia diagram of zircons from the quartz-fieldspathic breccia PC11. **b** Probability density distribution and histogram plot of U–Pb concordant zircon ages for the quartzitic sandstone PP1

221.5 ± 6.9 Ma (2σ, concordia age, MSWD = 1.7, $N = 5$). The latter age is similar to the weighted mean $^{206}Pb/^{238}U$ age yielded by the remaining four discordant zircon analyses (222 ± 32 Ma, 95% confidence level), which presumably reflect variable amounts of common Pb contamination and radiogenic Pb loss. We propose that the youngest concordant dates represent mixed domains including zircon portions that experienced Pb loss and/or common Pb contamination, i.e., they are not geologically meaningful.

8 Discussion

8.1 Age of the gabbroic crust from the Balagne ophiolite

The Balagne ophiolite preserves a primary Jurassic association of pillow and massive basalt lavas with ophiolitic

breccias and continent-derived quartzo-feldspathic clastic sediments. At the top of the succession, the pillow basalts are covered by Middle–Upper Jurassic pelagic sediments mostly consisting of radiolarian cherts. The basalt-sedimentary succession is tectonically associated with the Moltifao slice, which is composed of an intrusive sequence consisting of gabbronorites, oxide-rich gabbros and albitites, overlain by pillow basalt lavas.

U–Pb zircon geochronology indicates that the crystallization of the albitite from the Moltifao intrusive sequence occurred at 159 ± 3 Ma. Ophiolitic gabbros and leucocratic felsic rocks from the Schistes Lustrés Units of Alpine Corsica have been dated by U–Pb zircon geochronology at 158 ± 3 to 160 ± 2 Ma (2σ, Li et al. 2015, see also Fig. 2) and hence yielded similar ages. Li et al. (2015) proposed that the ophiolites from the Schistes Lustrés units formed in a more ocean-ward domain of the Liguria-Piedmont basin with respect to the Balagne ophiolite that was emplaced close to a continental margin. Mostly on the basis of field relationships, however, other authors considered the ophiolites from the Schistes Lustrés units as typical of an ocean-continent transition domain (Molli 2008; Molli and Malavieille 2011; Brovarone et al. 2011).

The U–Pb zircon age of 159 ± 3 Ma proposed for the formation of the Moltifao intrusive sequence is younger than the age of 169 ± 3 Ma proposed by Rossi et al. (2002) for a felsic dyke crosscutting an oxide-rich gabbro clast in the ophiolitic breccias. Two hypotheses can be formulated to explain the younger age of the Moltifao intrusive sequence with respect to the gabbro clasts in the breccias.

A first hypothesis implies that the Moltifao tectonic slice was part of a crustal sequence originally unrelated to the main basalt-sedimentary succession of the Balagne ophiolite and located in an oceanward sector of the Liguria-Piedmont basin. The Moltifao tectonic slice could therefore be paleographically analogous to the Pineto ophiolite, which is situated at the top of the Corsica Alpine tectonic stack and is devoid of high-pressure metamorphism, similar to the ophiolites from the Balagne region. The lower crust sequence of the Pineto ophiolite displays close structural and compositional similarities to lower crustal sections at slow and ultra-slow spreading ridges (Sanfilippo and Tribuzio 2013, 2015) and is crosscut by basalt dykes chemically similar to modern N-MORB basalts (Saccani et al. 2000). It is therefore conceivable that the Pineto ophiolite represents an oceanward sector of the Liguria-Piedmont basin. According to this hypothesis, in the Balagne ophiolite, the time lapse between the formation of a continent-near and an oceanward gabbroic sequence was 10 ± 6 Ma.

A second and alternative scenario implies that the Moltifao tectonic slice was originally physically contiguous to the main basalt-sedimentary succession of the Balagne ophiolite (i.e., the Moltifao intrusive sequence was part of the original basement of the main basalt-sedimentary succession of the Balagne ophiolite). According to this hypothesis, the Moltifao intrusive sequence and the intrusive rocks from the ophiolitic breccias would have similar crystallization ages. This hypothesis is consistent with the transitional MORB geochemical affinity of the Moltifao basalt lavas (Sanfilippo, unpublished PhD thesis), similar to the basalt lavas from the main basalt-sedimentary succession of the Balagne ophiolite (Venturelli et al. 1979), and would imply that the U–Pb zircon age of 169 ± 3 Ma reported by Rossi et al. (2002) was inaccurate. This age is a lower intercept obtained from mostly discordant analyses and is associated with a high MSWD (8.4) indicating a multiple distribution of U–Pb dates. The spread of $^{206}Pb/^{238}U$ zircon dates (Fig. 8), ranging from 175 ± 3 (2σ) to 163 ± 3 Ma (2σ), could reflect the incorporation of an inherited component in the oldest analyses, in agreement with the occurrence of: (1) Silurian and Neo-Archean zircons, and (2) a concordant U–Pb zircon date at 156 ± 2 (2σ) overlapping within error the U–Pb zircon age obtained in this work for the albitite (Fig. 8).

The second hypothesis also implies that the lower crust from the whole ophiolitic sequences of the Balagne region crystallized at 159 ± 3 Ma, i.e., within the Oxfordian according to the International Chronostratighraphic Chart (Cohen et al. 2013). However, the oldest radiolarian cherts from the main basalt-sedimentary succession of the Balagne ophiolite were dated as Late Bathonian to Early Callovian (Chiari et al. 2000; Bill et al. 2001; Peybernès et al. 2001), corresponding to the Unitary Association Zone

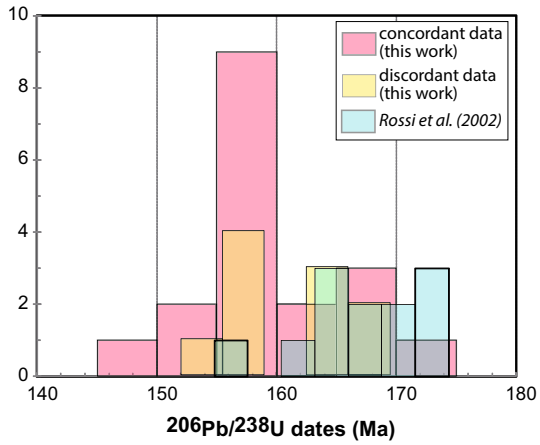

Fig. 8 Histogram plot of the $^{206}Pb/^{238}U$ zircon dates for the albitite GM1. $^{206}Pb/^{238}U$ zircon dates for a leucocratic felsic dyke from a gabbroic clast in the ophiolitic breccias obtained by Rossi et al. (2002) are reported for comparative purposes, $^{206}Pb/^{238}U$ dates of zircon interpreted by Rossi et al. (2002) as inherited grains were not plotted

(UAZ) seven of Baumgartner et al. (1995). The paradox of Oxfordian gabbros, younger than the deposition of early pelagic sediments, may be explained if radiolarite deposition would have taken place during ongoing magmatism, thereby implying that the radiolarites are locally older than magmatic products. We also wish to mention that gabbroic bodies having younger radiometric dates (~161 Ma) compared to biostrathigraphic dates of older overlying pelagic sediments (Lower Bathonian) have also been reported for other ophiolites of the Alpine-Apennine belt, such as the Ligurian Jurassic ophiolites (Tribuzio et al. 2016). Therefore, we cannot exclude an incorrect calibration of the biostratigraphic time-scale for the Middle–Upper Jurassic. Indeed, the temporal boundaries between Bathonian and Callovian (Middle Jurassic), between Callovian and Oxfordian (Middle–Upper Jurassic) and between Oxfordian and Kimmeridgian (Upper Jurassic) are not firmly constrained and markedly variable in the chronostrathigraphic scales proposed in the last fifteen years (cf. Gradstein et al. 2004; Pálfy et al. 2000). In addition, Danelian et al. (2008) showed the occurrence of a biostratigraphic incompatibility in a 7 m thick radiolarite sequence overlying the basalt pillow lavas from the Balagne ophiolite. Species of UAZ 8 (Mid Callovian-Early Oxfordian) and UAZ 9 (Mid-Late Oxfordian) are present in the same assemblage with species of UAZ 7, although they are not presumed to occur together in the zonation of Baumgartner et al. (1995). This indicates some uncertainties in the definition of the radiolarian ages for the sedimentary cover of the Balagne ophiolite. We conclude that there could not be substantial age differences regarding the formation of the lower oceanic crust in the Schistes Lustrés units and in the Moltifao intrusive sequence from the Balagne ophiolite.

8.2 Provenance of the quartzo-feldspathic clastic sediments

The quartzo-feldspathic breccia and the carbonate-rich quartzitic sandstone contain abundant grains of monocrystalline quartz with engulfed shape, which is typical of quartz of volcanic origin and therefore indicates the presence of a volcanic component in the source area. The occurrence of quartz grains preserving typical volcanic shape and the prevalence of zircons with sharp, sub-prismatic to prismatic habitus suggest that these quartzo-feldspathic clastic sediments have a low textural maturity, in agreement with their arkose whole-rock compositions. The quartzo-feldspathic clastic sediments rocks also contain subordinate sharp polygonal aggregates of quartz of metamorphic origin, which in tandem with the occurrence of rare clasts of white mica are consistent with the presence of metamorphic material in the source area. The concordant zircon date at 457 ± 15 Ma found in the quartzitic sandstone could be correlated with a minor contribution from the pre-Variscan metamorphic basement (Rossi et al. 1995; Renna and Tribuzio 2009).

U–Pb zircon geochronological data identified a homogeneous population for the quartzo-feldspathic breccia, with a mean U–Pb concordia age of 280 ± 2 Ma (Fig. 7a). A heterogeneous distribution of U–Pb zircon dates was obtained for the quartzitic sandstone, where we found a main peak at 279 ± 2 Ma that is statistically indistinguishable by the mean U–Pb zircon age yielded by the quartzo-feldspathic breccia. These ages are within error with the crystallization ages of 284 ± 4 and 278 ± 2 Ma obtained for ignimbrite rhyolites from Monte Cinto-Galeria volcanic sequences of Corsica (Rossi et al. 2015). Hence, the Balagne quartzo-feldspathic clastic sediments may have been supplied by volcanic material from the Corsica-Sardinia block. However, within the Permo-Carboniferous association composing the Sesia Magmatic System (western Alps, Sinigoi et al. 2010), which constitutes a virtually complete section of the Adriatic continental crust, the volcanic event was similarly dated by U–Pb zircon geochronology at 282 ± 3 Ma (Quick et al. 2009). In addition, the minor zircon components at 309 ± 7 Ma found in the quartzitic sandstone are similar to U–Pb zircon dates found in several intrusive and volcanic rocks associations from both Corsica (Paquette et al. 2003; Rossi et al. 2015) and Adriatic continental margins (Peressini et al. 2007; Renna and Tribuzio 2009). Note also that there are not significant geochronological differences between European and Adriatic continental margins with regards to the U–Pb zircon dates coeval to the zircon component at 262 ± 6 Ma found in the quartzitic sandstone, although there is no general consensus about their geological meaning (cf. Rossi et al. 2015; Dallagiovanna et al. 2009; Renna et al. 2007; Renna and Tribuzio 2009).

In summary, the U–Pb zircon geochronology of the quartzo-feldspathic clastic sediments re-inforces the view that Balagne ophiolite formed near a continent and that its quartzo-feldspathic clastic sediments were mainly supplied by volcanic material of Permian age. On the basis of the data reported in this study, the localization of the Balagne ophiolite in proximity to Europe rather than to the Adria margin cannot be unequivocally established.

9 Summary and concluding remarks

The Balagne ophiolite from central-northern Corsica is a continent-near fragment of oceanic lithosphere of the Jurassic Liguria-Piedmont basin. Pillow and massive basalt lavas are primarily associated with continental-derived quartzo-feldspathic sediments, and breccias with gabbro

and basalt clasts. The quartzo-feldspathic clastic sediments display a low degree of textural maturity and were derived from a source including SiO_2-rich volcanics and subordinate metamorphic material. U–Pb zircon geochronology identified a predominant ~280 Ma component, corresponding to the magmatic episodes developed during the Variscan orogenic collapse.

The ophiolitic breccias document that the marginal Balagne basalt-sedimentary succession was next to a topographic high mainly composed of a gabbroic sequence, presumably located in an oceanward position with respect to the continental margin (Marroni and Pandolfi 2007). The main basalt-sedimentary succession of the Balagne ophiolite is associated with a tectonic slice composed of an intrusive sequence dated at 159 ± 3 Ma and overlain by basalt lavas. The formation of the intrusive rocks from the tectonic slice from the Balagne ophiolite is contemporaneous with the ophiolitic gabbros from the adjacent Schistes Lustrés units (Li et al. 2015). On the basis of the U–Pb zircon dates obtained in this work and reported in the literature for the gabbroic clasts in the Balagne ophiolitic breccia (Rossi et al. 2002), the intrusive sequence from the tectonic slice could represent an oceanward sector of the Liguria-Piedmont basin younger than the gabbroic crust from the main basalt-sedimentary succession of the Balagne ophiolite. This hypothesis implies that the time interval intervened from continent-near to oceanward gabbroic crust formation was 10 ± 6 Ma. An alternative hypothesis implies that the intrusive sequence from the tectonic slice was part of the original basement of the main basalt-sedimentary succession of the Balagne ophiolite and therefore had similar crystallization age to the intrusive rocks from the ophiolitic breccia.

Acknowledgments We are grateful to A. von Quadt, M. Marroni and editor S. Schmid for the constructive comments that considerably improved the quality of this study.This work was financially supported by Università degli Studi di Pavia.

References

Anders, E., & Ebihara, M. (1982). Solar system abundances of the elements. *Geochimica et Cosmochimica Acta, 46,* 2363–2380.

Baud, J.P. (1975). Étude géologique du massif de roches vertes de Haute-Balagne (Corse). PhD thesis.

Baud, J. P., & Rollet, M. (1973). Mode de gisement des roches vertes et structure de la Haute Balagne, Corse. *Annales Scientifiques de l'Université de Besançon, Series, 3*(19), 267–279.

Baumgartner, P.O., Bartolini, A., Carter, E.S., Conti, M., Cortese, G., Danelian, T., De Wever, P., Dumitrica, P., Dumitrica-Jud, R., Gorican, S., Guex, J., Hull, D.M., Kito, N., Marcucci, M., Matsuoka, A., Murchey, B., O'Dogherty, L., Savary, J., Vishnevskaya, V., Widz, D., & Yao, A. (1995). Middle Jurassic to Early Cretaceous radiolarian biochronology of Tethys based on Unitary Associations. In: InterRad Jurassic-Cretaceous Working Group (Ed.), "Middle Jurassic to Lower Cretaceous Radiolaria of Tethys: Occurrences, Systematics, Biochronology". Memoires de Geologie (Lausanne) p 23.

Beltrando, M., Manatschal, G., Mohn, G., Dal Piaz, G. V., Brovarone, A. V., & Masini, E. (2014). Recognizing remnants of magma-poor rifted margins in high-pressure orogenic belts: The Alpine case study. *Earth-Science Reviews, 131,* 88–115.

Bill, M., Bussy, F., Cosca, M., Masson, H., & Hunziker, J. C. (1997). High-precision U-Pb and 40Ar/39Ar dating of an Alpine ophiolite (Gets nappe, French Alps). *Eclogae Geologicae Helvetiae, 90,* 43–54.

Bill, M., O'Dogherty, L., Guex, J., Baumgartner, P. O., & Masson, H. (2001). Radiolarite ages in Alpine-Mediterranean ophiolites: Constraints on the oceanic spreading and the Tethys-Atlantic connection. *Geological Society of America Bulletin, 113,* 129–143.

Borsi, L., Schärer, U., Gaggero, L., & Crispini, L. (1996). Age, origin and geodynamic significance of plagiogranites in lherzolites and gabbros of the Piedmont-Ligurian ocean basin. *Earth and Planetary Science Letters, 140,* 227–241.

Bortolotti, V., Cellai, D., Chiari, M., Vaggelli, G., & VIlla, I. M. (1995). 40Ar/39Ar dating of Apenninic ophiolites: 3. Plagiogranites from Sasso di Castro, Northern Tuscany, Italy. *Ofioliti, 20,* 55–65.

Bracciali, L., Marroni, M., Luca, P., & Sergio, R. (2007). Geochemistry and petrography of Western Tethys Cretaceous sedimentary covers (Corsica and Northern Apennines): from source areas to configuration of margins. *Geological Society of America Special Papers, 420,* 73–93.

Brovarone, A. V., Beltrando, M., Malavieille, J., Giuntoli, F., Tondella, E., Groppo, C., et al. (2011). Inherited ocean–continent transition zones in deeply subducted terranes: insights from Alpine Corsica. *Lithos, 124*(3), 273–290.

Chiari, M., Marcucci, M., & Principi, G. (2000). The age of the radiolarian cherts associated with the ophiolites in the Apennines (Italy). *Ofioliti, 25,* 141–146.

Cohen, K. M., Finney, S. C., Gibbard, P. L., & Fan, J. X. (2013). The ICS international chronostratigraphic chart. *Episodes, 36,* 199–204.

Costa, S., & Caby, R. (2001). Evolution of the Ligurian Tethys in the Western Alps: Sm/Nd and U/Pb geochronology and rare-earth element geochemistry of the Montgenevre ophiolite (France). *Chemical Geology, 175,* 449–466.

Dallagiovanna, G., Gaggero, L., Maino, M., Seno, S., & Tiepolo, M. (2009). U–Pb zircon ages for post-Variscan volcanism in the Ligurian Alps (northern Italy). *Journal of the Geological Society of London, 166,* 101–114.

Danelian, T., De Wever, P., & Durand-Delga, M. (2008). Revised radiolarian ages for the sedimentary cover of the Balagne ophiolite (Corsica, France). Implications for the palaeoenvironmental evolution of the Balano-Ligurian margin. *Bulletin de la Societe Geologique de France, 179,* 289–296.

Durand-Delga, M. (1984). Principaux traits de la Corse Alpine et corrélations avec les Alpes Ligures. *Memorie della Società Geologica Italiana, 28,* 285–329.

Durand-Delga, M., Lahondère, D., Puccinelli, A., Rossi, P., & Vellutini, P. (2001). Pre-Meeting transect Corsica-Elba Island Southern Tuscany Guidebook-Corsica. *Ofioliti, 26,* 303–320.

Durand-Delga, M., Peybernès, B., & Rossi, P. (1997). Arguments en faveur de la position, au Jurassique, des ophiolites de Balagne (Haute-Corse, France) au voisinage de la marge continentale européenne. *Comptes Rendus de l'Académie des Sciences-Series IIA-Earth and Planetary Science, 325*(12), 973–981.

Gradstein, F. M., Ogg, J. G., & Smith, A. G. (2004). *A geologic time scale 2004 (Vol. 86)*. Cambridge: Cambridge University Press.

Grimes, C. B., John, B. E., Cheadle, M. J., Mazdab, F. K., Wooden, J. L., Swapp, S., et al. (2009). On the occurrence, trace element geochemistry, and crystallization history of zircon from in situ

ocean lithosphere. *Contributions to Mineralogy and Petrology, 158,* 757–783.

Grimes, C. B., Ushikubo, T., John, B. E., & Valley, J. W. (2011). Uniformly mantle-like δ18O in zir- cons from oceanic plagiogranites and gabbros. *Contributions to Mineralogy and Petrology, 161,* 13–33.

Gromet, L. P., Dymek, R. F., Haskin, L. A., & Korotev, R. L. (1984). The "North American shale composite": its compilation, major and trace element characteristics. *Geochimica et Cosmochimica Acta, 48,* 2469–2482.

Gruppo di Lavoro sulle Ofioliti Mediterranee. (1977). I complessi ofiolitici e le unità cristalline della Corsica alpina. *Ofioliti, 2,* 265–324.

Herron, M. M. (1988). Geochemical classification of terrigenous sands and shales from core or log data. *Journal of Sedimentary Research, 58*(5), 820–829.

Jackson, S. E., Pearson, N. J., Griffin, W. L., & Belousova, E. A. (2004). The application of laser ablation-inductively coupled plasma-mass spectrometry to in situ U–Pb zircon geochronology. *Chemical Geology, 211,* 47–69.

Kaczmarek, M.-A., Müntener, O., & Rubatto, D. (2008). Trace element chemistry and U–Pb dating of zircons oceanic gabbros and their relationship with whole rock composition (Lanzo, Italian Alps). *Contributions to Mineralogy and Petrology, 155,* 295–312.

Kretz, R. (1983). Symbols for rock-forming minerals. *American mineralogist, 68,* 277–279.

Lagabrielle, Y., & Cannat, M. (1990). Alpine Jurassic ophiolites resemble the modern central Atlantic basement. *Geology, 18,* 319–322.

Li, X. H., Faure, M., Lin, W., & Manatschal, G. (2013). New isotopic constraints on age and magma genesis of an embryonic oceanic crust: the Chenaillet Ophiolite in the Western Alps. *Lithos, 160,* 283–291.

Li, X. H., Faure, M., Rossi, P., Lin, W., & Lahondere, D. (2015). Age of Alpine Corsica ophiolites revisited: Insights from in situ zircon U–Pb age and O–Hf isotopes. *Lithos, 220,* 179–190.

Liati, A., Froitzheim, N., & Fanning, C. M. (2005). Jurassic ophiolites within the Valais domain of the Western and Central Alps: geochronological evidence for re-rifting of oceanic crust. *Contributions to Mineralogy and Petrology, 149,* 446–461.

Lombardo, B., Rubatto, D., & Castelli, D. (2002). Ion microprobe U–Pb dating of zircon from a Monviso metaplagiogranite: implications for the evolution of the Piedmont-Liguria Tethys in the Western Alps. *Ofioliti, 27,* 109–117.

Ludwig, K. R. (2003). *Isoplot/Ex: Special Publication No. 4*. Berkeley: Berkeley Geochronology Center.

Malavieille, J., Chemenda, A., & Larroque, C. (1998). Evolutionary model for Alpine Corsica: mechanism for ophiolite emplacement and exhumation of high-pressure rocks. *Terra Nova, 10,* 317–322.

Manatschal, G., & Müntener, O. (2009). A type sequence across an ancient magma-poor ocean–continent transition: the example of the western Alpine Tethys ophiolites. *Tectonophysics, 473,* 4–19.

Manatschal, G., & Nievergelt, P. (1997). A continent–ocean transition recorded in the Err and Platta nappes (Eastern Switzerland). *Eclogae Geologicae Helvetiae, 90,* 3–27.

Marroni, M., Molli, G., Montanini, A., & Tribuzio, R. (1998). The association of continental crust rocks with ophiolites in the Northern Apennines (Italy): implications for the continent-ocean transition in the Western Tethys. *Tectonophysics, 292,* 43–66.

Marroni, M., Molli, G., Pandolfi, L., Piccardo, G.B., Principi, G., Saccani, E., Tribuzio, R., & Garfagnoli, F. (2007). The Alpine Corsica ophiolite field trip: the primary features, the tectonometamorphic orogenic imprint and the relationships with the continental units. GLOM (Working group of Mediterranean Ophiolite), Vol. Field Trip- guide book, GLOM (Working group of Mediterranean Ophiolite)-Corsica (Francia), pp. 1–65.

Marroni, M., & Pandolfi, L. (2003). Deformation history of the ophiolite sequence from the Balagne Nappe, northern Corsica: insights in the tectonic evolution of Alpine Corsica. *Geological Journal, 38,* 67–83.

Marroni, M., & Pandolfi, L. (2007). The architecture of an incipient oceanic basin: a tentative reconstruction of the Jurassic Liguria-Piemonte basin along the Northern Apennines-Alpine Corsica transect. *International Journal of Earth Science, 96,* 1059–1078.

Molli, G. (2008). Northern Apennine–Corsica orogenic system: an updated overview. *Geological Society, London, Special Publications, 298,* 413–442.

Molli, G., & Malavieille, J. (2011). Orogenic processes and the Corsica/Apennines geodynamic evolution: insights from Taiwan. *International Journal of Earth Sciences, 100,* 1207–1224.

Montanini, A., Tribuzio, R., & Anczkiewicz, R. (2006). Exhumation history of a garnet pyroxenite-bearing mantle section from a continent–ocean transition (Northern Apennine ophiolites, Italy). *Journal of Petrology, 47,* 1943–1971.

Müntener, O., Pettke, T., Desmurs, L., Meier, M., & Schaltegger, U. (2004). Refertilization of mantle peridotite in embryonic ocean basins: trace element and Nd isotopic evidence and implications for crust–mantle relationships. *Earth and Planetary Science Letters, 221,* 293–308.

Ohnenstetter, M., Ohnenstetter, D., Vidal, P., Cornichet, J., Hermitte, D., & Mace, J. (1981). Crystallization and age of zircon from Corsican ophiolitic albitites: consequences for oceanic expansion in Jurassic times. *Earth and Planetary Science Letters, 54,* 397–408.

Pálfy, J., Smith, P. L., & Mortensen, J. K. (2000). A U–Pb and $^{40}Ar/^{39}Ar$ time scale for the Jurassic. *Canadian Journal of Earth Sciences, 37,* 923–944.

Paquette, J.-L., Ménot, R.-P., Pin, C., & Orsini, J.-B. (2003). Episodic and short-lived granitic pulses in a post-collisional setting: evidence from precise U–Pb zircon dating through a crustal cross-section in Corsica. *Chemical Geology, 198,* 1–20.

Paton, C., Hellstrom, J., Paul, B., Woodhead, J., & Hergt, J. (2011). Iolite: freeware for the visualisation and processing of mass spectrometric data. *Journal of Analytical Atomic Spectrometry, 26,* 2508–2518.

Paton, C., Woodhead, J. D., Hellstrom, J. C., Hergt, J. M., Greig, A., & Maas, R. (2010). Improved laser ablation U–Pb zircon geochronology through robust downhole fractionation correction. *Geochemistry, Geophysics, Geosystems, 11,* Q0AA06.

Peressini, G., Quick, J. E., Sinigoi, S., Hofmann, A. W., & Fanning, M. (2007). Duration of a large mafic intrusion and heat transfer in the lower crust: a SHRIMP U–Pb zircon study in the Ivrea–Verbano Zone (Western Alps, Italy). *Journal of Petrology, 48,* 1185–1218.

Peybernès, B., Durand-Delga, M., & Cugny, P. (2001). Reconstitution, en Corse, au Jurassique moyen–supérieur, de la marge européenne de l'océan Liguro-Piémontais, grâce à des niveaux repères à Praekurnubia crusei (foraminifère). *Comptes Rendus de l' Academie des Sciences Serie IIa, 332,* 499–506.

Quick, J. E., Sinigoi, S., Peressini, G., Demarchi, G., Wooden, J. L., & Sbisa, A. (2009). Magmatic plumbing of a large Permian caldera exposed to a depth of 25 km. *Geology, 37,* 603–606.

Rampone, E., Hofmann, A. W., Piccardo, G. B., Vannucci, R., Bottazzi, P., & Ottolini, L. (1995). Petrology, mineral and isotope geochemistry of the External Liguride peridotites (Northern Apennines, Italy). *Journal of Petrology, 36,* 81–105.

Renna, M. R., & Tribuzio, R. (2009). Petrology, geochemistry and U–Pb zircon geochronology of lower crust pyroxenites from northern Apennine (Italy): insights into the post-collisional Variscan evolution. *Contributions to Mineralogy and Petrology, 157,* 813–835.

Renna, M. R., Tribuzio, R., & Tiepolo, M. (2007). Origin and timing of the post-Variscan gabbro–granite complex of Porto (Western Corsica). *Contributions to Mineralogy and Petrology, 154,* 493–517.

Rossi, P., Cocherie, A., & Durand-Delga, M. (1995). Geochronological evidence on the presence of Panafrican basement in Western Corsica (France): Constraints on the palaeogeography of the south European Variscan orogen. Comptes Rendus de l'Academie des Sciences. Serie 2. *Sciences de la Terre et des Planetes, 321,* 983–992.

Rossi, P., Cocherie, A., & Fanning, C. M. (2015). Evidence in Variscan Corsica of a brief and voluminous Late Carboniferous to Early Permian volcanic-plutonic event contemporaneous with a high-temperature/low-pressure metamorphic peak in the lower crust. *Bulletin de la Société Géologique de France, 186,* 171–192.

Rossi, P., Cocherie, A., Lahondère, D., & Fanning, C. M. (2002). La marge européenne de la Téthys jurassique en Corse: datation de trondhjémites de Balagne et indices de croûte continentale sous le domaine Balano-Ligure. *Comptes Rendus Geoscience, 334,* 313–322.

Rossi, P., & Durand-Delga, M. (2001). Significance of sandstones interbedded in the Jurassic basalts of the Balagne ophiolitic nappe (Corsica, France). *Ofioliti, 26,* 169–174.

Rossi, P., Durand-Delga, M., & Lahondere, J. C. (2001). Carte Géologique de France (1/50000), feuille Santo-Pietro-di-Tenda (1106). In: Rossi, P., Durand-Delga, M., Lahondere, J. C. & Lahondere, D (Eds.), Orleans BRGM. Notice explicative par (p. 224). Orléans: BRGM Orléans.

Rubatto, D., Gebauer, D., & Fanning, M. (1998). Jurassic formation and Eocene subduction of the Zermatt–Saas-Fee ophiolites: implications for the geodynamic evolution of the Central and Western Alps. *Contributions to Mineralogy and Petrology, 132,* 269–287.

Rubatto, D., & Hermann, J. (2003). Zircon formation during fluid circulation in eclogites (Monviso, Western Alps): implications for Zr and Hf budget in subduction zones. *Geochimica et Cosmochimica Acta, 67,* 2173–2187.

Rubatto, D., Müntener, O., Barnhoorn, A., & Courtney, G. (2008). Dissolution–reprecipitation of zircon at low-temperature, high-pressure conditions (Lanzo Massif, Italy). *American Mineralogist, 93,* 1519–1529.

Rubatto, D., & Scambelluri, M. (2003). U–Pb dating of magmatic zircon and metamorphic baddeleyite in the Ligurian eclogites (Voltri Massif, Western Alps). *Contributions to Mineralogy and Petrology, 146,* 341–355.

Saccani, E., Dilek, Y., Marroni, M., & Pandolfi, L. (2015). Continental margin ophiolites of Neotethys: Remnants of ancient Ocean-Continent Transition Zone (OCTZ) lithosphere and their geochemistry, mantle sources and melt evolution patterns. *Episodes, 38,* 230–249.

Saccani, E., Padoa, E., & Tassinari, R. (2000). Preliminary data on the Pineto gabbroic Massif and Nebbio basalts: progress toward the geochemical characterization of Alpine Corsica ophiolites. *Ofioliti, 25,* 75–85.

Saccani, E., Principi, G., Garfagnoli, F., & Menna, F. (2008). Corsica ophiolites: geochemistry and petrogenesis of basaltic and metabasaltic rocks. *Ofioliti, 33,* 187–207.

Sanfilippo, A., & Tribuzio, R. (2013). Building of the deepest crust at a fossil slow-spreading centre (Pineto gabbroic sequence, Alpine Jurassic ophiolites). *Contributions to Mineralogy and Petrology, 165,* 705–721.

Sanfilippo, A., Tribuzio, R., Tiepolo, M., & Berno, D. (2015). Reactive flow as dominant evolution process in the lowermost oceanic crust: evidence from olivine of the Pineto ophiolite (Corsica). Contributions to Mineralogy and Petrology, *170*, 1–12.

Schaltegger, U., Desmurs, L., Manatschal, G., Müntener, O., Meier, M., Frank, M., et al. (2002). The transition from rifting to seafloor spreading within a magma-poor rifted margin: field and isotopic constraints. *Terra Nova, 14,* 156–162.

Schoene, B. (2014). 4.10–U–Th–Pb geochronology. Treatise on geochemistry, Second Editionth edn. Elsevier, Oxford, 341–378.

Schwartz, J. J., John, B. E., Cheadle, M. J., Wooden, J. L., Mazdab, F., Swapp, S., et al. (2010). Dissolution–reprecipitation of igneous zircon in mid-ocean ridge gabbro, Atlantis Bank, Southwest Indian Ridge. *Chemical Geology, 274,* 68–81.

Sinigoi, S., Quick, J.E., Demarchi, G., & Peressini, G. (2010). The Sesia magmatic system. In: Beltrando, M., Peccerillo, A., Mattei, M., Conticelli, S., Doglioni, C. (Eds.), Journal of the Virtual Explorer, 36, 1–33.

Stucki, A., Rubatto, D., & Trommsdorff, V. (2003). Mesozoic ophiolite relics in the Southern Steep Belt of the Central Alps. *Swiss Bulletin of Mineralogy and Petrology, 83,* 285–299.

Tiepolo, M. (2003). In situ Pb geochronology of zircon with laser ablation–inductively coupled plasma–sector field mass spectrometry. *Chemical Geology, 199,* 159–177.

Tribuzio, R., Garzetti, F., Corfu, F., Tiepolo, M., & Renna, M. R. (2016). U–Pb zircon geochronology of the Ligurian ophiolites (Northern Apennine, Italy): Implications for continental breakup to slow seafloor spreading. *Tectonophysics, 666,* 220–243.

Tribuzio, R., Renna, M. R., Dallai, L., & Zanetti, A. (2014). The magmatic–hydrothermal transition in the lower oceanic crust: Clues from the Ligurian ophiolites, Italy. *Geochimica et Cosmochimica Acta, 130,* 188–211.

Venturelli, G., Capedri, S., Thorpe, R. S., & Potts, P. J. (1979). Rare-earth and other element distribution in some ophiolitic metabasalts of Corsica, Western Mediterranean. *Chemical Geology, 24,* 339–353.

Von Quadt, A., Gallhofer, D., Guillong, M., Peytcheva, I., Waelle, M., & Sakata, S. (2014). U–Pb dating of CA/non-CA treated zircons obtained by LA-ICP-MS and CA-TIMS techniques: impact for their geological interpretation. *Journal of Analytical Atomic Spectrometry, 29,* 1618–1629.

Wiedenbeck, M., Alle, P., Corfu, F., Griffin, W. L., Meier, M., Oberli, F., et al. (1995). Three natural zircon standards for U–Th–Pb, Lu–Hf, trace elements ad REE analyses. *Geostandards Newsletter, 19,* 1–23.